Joint PAPR and OBP Reduction for NC-OFDM Systems

Hsuan-Fu Wang[2], Fang-Biau Ueng[1] and Bo-Heng Yeh[1]

***Abstract*—**The spectrum resource is always a critical issue for wireless communications since it directly impacts the data rate and capacity. However, the problem of spectrum resource scarcity always exists. Moreover, spectrum resource scarcity becomes more severe as new communication technologies and wireless applications sprout. Noncontiguous orthogonal frequency division multiplexing (NC-OFDM) is a multicarrier method for bandwidth utilization. Unfortunately, this system has two fatal defects: high peak-to-average power ratio (PAPR) and considerable out-of-band power (OBP), which are detrimental to the system's performance. To solve these two problems, we propose a convex optimization-based method for joint PAPR and OBP reduction in NC-OFDM Systems. The strategy is to permit the secondary user to utilize the unoccupied spectrum of the primary user with dynamic spectrum sharing (DSS) based on a cognitive radio network (CRN). To this end, a flexible system operating over noncontiguous bands and DSS scenarios is necessary. The simulation results have shown that our method could effectively improve the overall performance and outperform other schemes, i.e., projections onto convex sets (POCS) and alternating projections onto convex and non-convex sets (APOCNCS), without harming the transmission of the primary system. The collaboration between secondary and primary systems is viable with the proposed method.

***Index Terms*—**NC-OFDM, DSS, CRN, PAPR, OBP, POCS, APOCNCS.

I. Introduction

SPECTRUM congestion is always a thorny issue, especially in mobile wireless communication. As innovative technologies and applications develop rapidly, more spectrum resources are required, creating a more complex spectrum resource scarcity [1]. Since the bandwidth directly dominates the data rate and capacity, which is a part of spectrum resources, it urges to address the shortage of spectrum resources and ease the congestion. The most effective solution is to transmit GHz to THz levels [2] over higher frequency bands with a much more comprehensive range of available bandwidth. Unfortunately, the signals transmitted over these bands would suffer more severe attenuation than the currently employed bands, and acquiring the license or permission for the spectrum resource would be an extra expenditure. Therefore, a more practical and economical way is to increase the spectrum utilization efficiency (SUE) within finite bandwidth by dynamic spectrum sharing (DSS) based on cognitive radio network (CRN) [3]-[5]. The CRN can sense the spectrum information, detect the states of frequency bands, and dynamically allocate the spectrum resource to realize DSS.

In the fifth generation (5G) mobile wireless communication network, orthogonal frequency division multiplexing (OFDM) has been designated standard modulation [6]. OFDM is an omnipresent system due to its irreplaceable features, such as robustness against multipath fading and uncomplicated equalization. Many OFDM variants have been proposed to fit different circumstances. One of them, noncontiguous OFDM (NC-OFDM), can be regarded as OFDM with spectrum sensing-based cognitive radio (CR). NC-OFDM enables a secondary user (SU) to employ unoccupied subcarriers belonging to the primary user (PU), thus enhancing the SUE [7]. Since NC-OFDM could be operated over noncontiguous frequency bands, this system is a flexible choice for SU to cooperate with the primary system; it is suitable for future wireless communication [8]. Moreover, NC-OFDM's high flexibility and adaptability are desirable and indispensable for the upcoming generation of wireless communications, such as beyond 5G (B5G) and the sixth generation (6G) [9].

However, NC-OFDM is cursed with a high peak-to-average power ratio (PAPR) and considerable out-of-band power (OBP) [10]. The former is a common challenge for multicarrier transmission. While multiple orthogonal subcarriers overlap through Fast Fourier transform/Inverse Fast Fourier transform (FFT/IFFT), the time domain signal might have spikes that cause strong amplitude fluctuations. If we input a signal with a large PAPR to the power amplifier (PA), the PA would most likely work in a nonlinear region depending on the saturation power of the PA and introduce harmonic distortion and intermodulation distortion [11]. The latter, OBP, is the power of sidelobes outside their frequency bands' scope. Generally, the pulse-shaping function dominates the magnitude of sidelobes. The pulse shaping function is rectangular for OFDM-based systems with a Sinc function frequency response. Because the Sinc function decays slowly, high-level sidelobes exist in the frequency domain. These redundant sidelobes would waste transmit power and interfere with the adjacent channels. Various joint PAPR and OBP reduction methods have been published in the literature to overcome the defects mentioned above. A precoding scheme to jointly reduce PAPR values in the SUs spectrum band and suppress sidelobes of

[1]The authors are with the Department of Electrical Engineering, National Chung Hsing University, Taichung, Taiwan. (e-mail: fbueng@nchu.edu.tw, strikecv47@gmail.com). [2]The author is with Department of Aeronautical Engineering, National Formosa University, Yunlin, Taiwan. (e-mail: hfwang@nfu.edu.tw). This work was supported in part by the Ministry of Science and Technology of Taiwan under Contract NSTC 112-2221-E-005-063. (Corresponding author: Fang-Biau Ueng).

signals in the PU band for the CR system with NC-OFDM is presented in [12]. A joint method for the PAPR reduction and sidelobe suppression is based on the partial transmit sequence (PTS) method, and the objective is modeled as an optimization problem to minimize PAPR with a constraint on the maximum tolerable sidelobe power in [13]. The literature [14] proposed a novel joint suppression method of PAPR and sidelobe power of hybrid carrier (HC) system based on weighted-type fractional Fourier transform (WFRFT) with flexible selections of WFRFT parameter α, shaping parameter β, and windowing parameter γ is employed for multi-objective optimization of the proposed HC framework.

A time-domain iterative algorithm combining time-domain N-continuous OFDM (TD-NC-OFDM) and serial peak cancellation (SPC), aiming at solving both the spectral leakage and PAPR problems to optimize 5G multicarrier waveforms and the projections onto convex sets (POCS) algorithm was applied to prove the effectiveness of the iterative program in the proposed algorithm in [10]. Correlative precoders are designed in [15] to endow correlatively precoded OFDM waveforms with reduced PAPR while preserving enhanced intercarrier interference (ICI) self-cancelation or improved spectral sidelobe suppression, respectively, or jointly. The method aims at the joint utilization of extending the outer constellation points and adding pre-determined tones onto the subcarriers to reduce both PAPR and sidelobe power jointly proposed in [16]. A joint model that efficiently suppresses both PAPR and spectral leakage by combining SPC and TD-NC-OFDM is proposed [17]. To jointly reduce the sidelobe power of signals in licensed user (LU) bands and PAPR for the CR system with the NC-OFDM scheme, a scheme that combines the precoding matrix with the multiple choice sequences (MCS) technique using different pseudo-random sequence assignments is proposed in [18]. To suppress the in-band-out-of-subband (IBOSB) radiation jointly and high PAPR in orthogonal frequency division multiplexing access (OFDMA) systems, a precoding scheme that is ahead of inverse discrete Fourier transformation (IDFT) is presented in [19].

There are four prominent schemes proposed in recent years, including signal cancellation (SC) [20], suppressing alignment (SA) [21], alternating POCS [22], and alternating projections onto convex and non-convex sets (APOCNCS) [23]. The SC method dynamically extends the SU subcarriers, which bear outer constellation data symbols, and overlays the PU subcarriers with cancellation signals [20]. The outer constellation symbols represent the corner and boundary points in the digital modulation constellation. For instance, 16 Quadrature amplitude modulation (QAM) has twelve outer constellation symbols. Extending SU subcarriers and generating cancellation signals can be realized by solving the optimization problem formulated in [20]. Although SC can achieve good PAPR and OBP performance under 4-QAM and 16-QAM, it is notable that this method might be ineffective in high-order modulation since the proportion of outer constellation points to all constellation points decreases as the modulation order rises. For SA, the suppressing and data signals are amalgamated into the OFDM signals and discarded when the cyclic prefix (CP) is removed at the receiving end [21]. The suppressing signal is carefully designed to attain two goals. One is to minimize the OBP and PAPR, and the other is to avoid posing additional interference when recovering data in the receiver. The channel state information (CSI) must be available at the transmitter to achieve the second one. Specifically, a part of the suppressing signal is constructed of the null space of the channel matrix, and it would be automatically eliminated when passing through the channel. As for the first goal, the sum of OBP and PAPR multiplied by a weighting factor is the objective function. Incidentally, the weighting factor is used for adjusting the reduction gain of PAPR and OBP. Finally, the suppressing signal can be obtained by minimizing the objective function with a power constraint. Even though SA could reduce PAPR and OBP without losing spectrum efficiency and error rate, it can't be operated without CSI, making this scheme impractical in many general scenarios. A large portion of unoccupied subcarriers is assigned to SU for data transmission, and PU subcarriers and the rest of the unoccupied subcarriers accommodate the adjusting weights [22]. The adjusting weights are used for joint PAPR and OBP reduction, which can be obtained by the POCS algorithm [22]. At first, this method initializes the input vector with SU's data and constructs two convex sets, OBP and PAPR sets, which correspond to OBP and peak power limitations, respectively. Secondly, the input vector would be projected onto the two convex sets in order of priority. For example, we project the input vector onto the OBP positioned after the project onto the PAPR set if the OBP reduction has priority over the PAPR reduction. The third step updates the input vector with the current output and returns to the second step. This algorithm will operate the second and third steps iteratively until reaching the vector point or iteration limit. Finally, the optimal output of POCS will be the discrete frequency domain NC-OFDM signal.

In contrast with POCS, APOCNCS [23] creates a non-convex set to increase the in-band power (IBP) and projects the input vector onto this set before projecting onto the two convex sets of POCS. The procedure of APOCNCS is almost the same as POCS; they are essentially based on the alternating projection method, which is prevalent and has been applied in many fields. POCS and APOCNCS can effectively achieve the primary requirement, but the minor one cannot be guaranteed. Moreover, the data of PU might be seriously interfered with by the available adjusting weights on PU subcarriers, which is prohibited in DSS scenarios.

To alleviate the performance of NC-OFDM without degrading the transmission quality of PU, we proposed a joint PAPR and OBP reduction method that can significantly decrease the PAPR and OBP by leveraging convex optimization techniques. The contributions of this study include:

- Two algorithms that utilize Lagrangian multipliers and Karush-Kuhn-Tucker (KKT) conditions are proposed to reduce PAPR and OBP for the NC-OFDM system;
- The proposed algorithms are investigated by mathematical analysis and validated by simulation;
- The computation complexity of the proposed method is lower than those of POCS and APOCNCS schemes.

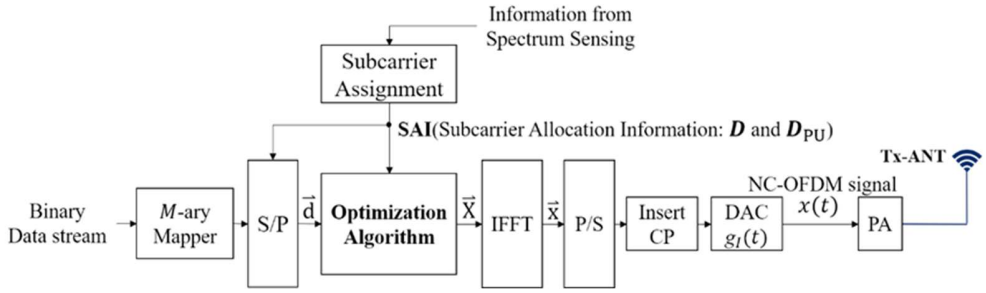

Fig. 1. The NC-OFDM Transmitter.

This paper is organized as follows. The NC-OFDM transmitter, OBP, PAPR, and receiver are described in Section II. Section III presents the proposed optimization method's design criteria, two algorithms, and mathematical analysis. The simulation results are illustrated in Section IV. Finally, the conclusion is presented in Section V.

II. System Model

A. Transmitter

Considering that there are N subcarriers in the licensed spectrum and PU currently occupies a part of them, we divide the unoccupied/vacant subcarriers into two parts: SU subcarriers and adjusting subcarriers. SU employs the SU subcarriers for data transmission. The adjusting subcarriers and all PU subcarriers are used to accommodate PAPR and OBP reduction variables. The NC-OFDM transmitter is depicted in **Fig. 1**. Let $\boldsymbol{D}$ and $\boldsymbol{D}_{\text{PU}}$ be the SU and PU subcarriers' index sets. Note that S/P and P/S are serial to parallel conversion parallel to serial conversion, respectively. The data vector of SU after subcarrier allocation is given by

$$\vec{\mathrm{d}} = \left[d_0 \; d_1 \cdots d_{N-1}\right]^{\mathrm{T}}, \; d_k = 0 \text{ for all } k \notin \boldsymbol{D}, \tag{1}$$

where $(.)^{\mathrm{T}}$ denotes the transpose of a matrix or vector. Note that the SU and PU subcarriers are disjoint (i.e. $\boldsymbol{D} \cap \boldsymbol{D}_{\text{PU}} = \varnothing$). The data vector and subcarrier allocation information (SAI) is subsequently sent to the proposed algorithm. The discrete frequency domain NC-OFDM signal is the output of the proposed algorithm, and we denote it by

$$\vec{\mathrm{X}} = \left[X_0 \; X_1 \cdots X_{N-1}\right]^{\mathrm{T}} \tag{2}$$

After passing $\vec{\mathrm{X}}$ through the IFFT, we have the discrete-time NC-OFDM signal as

$$\vec{\mathrm{x}} = \mathbf{F}^{-1}\vec{\mathrm{X}} = \left[x_0 \; x_1 \cdots x_{N-1}\right]^{\mathrm{T}}, \tag{3}$$

where $\mathbf{F}$ and $\mathbf{F}^{-1}$ are defined as the DFT/IDFT matrices. The elements in (3) are defined as

$$\vec{\mathrm{x}} = \mathbf{F}^{-1}\vec{\mathrm{X}} = \left[x_0 \; x_1 \cdots x_{N-1}\right]^{\mathrm{T}}, \tag{4}$$

With the discrete-time NC-OFDM signal, the continuous-time OFDM signal $x(t)$ can be produced by inserting CP and passing through an interpolation filter/digital-to-analog converter (DAC).

$$x(t) = g_I(t) * \left[\sum_{n=-N_{cp}}^{N-1} x_n \delta(t - nT_s)\right], \tag{5}$$

where $g_I(t)$ is the impulse response of interpolation filter/DAC, $*$ is convolution operation, T_s is the sampling period, N_{cp} denotes the CP length, and $\delta(t - nT_S)$ is the unit impulse function.

B. Out-of-Band Power

By operating the Fourier transform (FT), we obtain the frequency response of the NC-OFDM signal

$$X(f) = \mathscr{F}\left\{x(t)\right\} = G_I(f)\left[\sum_{n=-N_{cp}}^{N-1} x_n e^{-j2\pi n T_s f}\right], \tag{6}$$

where $\mathscr{F}\{.\}$ denotes the FT operation and $G_I(f) = \mathscr{F}\left\{g_I(t)\right\}$. Substituting (4) into (6), we have

$$X(f) = \frac{1}{\sqrt{N}} G_I(f) \sum_{k=0}^{N-1} X_k \left[\sum_{n=-N_{cp}}^{N-1} e^{j2\pi\left(\frac{k}{N} - T_s f\right)n}\right] \tag{7}$$

The geometric series in (7) can be simplified as

$$\sum_{n=-N_{cp}}^{N-1} e^{j2\pi\left(\frac{k}{N} - T_s f\right)n} = \frac{\sin\left(\frac{\varphi}{2}L\right)}{\sin\left(\frac{\varphi}{2}\right)} e^{j\frac{\varphi}{2}\left(L - 2N_{cp} - 1\right)}, \tag{8}$$

where $\varphi = 2\pi\left[(k/N) - T_s f\right]$, and $L = N + N_{cp}$ is the symbol length of the NC-OFDM signal (after CP insertion). While $(\varphi / 2\pi) \in \mathrm{Z}$ (set of integers), (8) would be undefined. We invoke L'Hospital's Rule, and the result is

$$\lim_{\varphi \to 0} \frac{\sin\left(\frac{\varphi}{2}L\right)}{\sin\left(\frac{\varphi}{2}\right)} e^{j\frac{\varphi}{2}\left(L - 2N_{cp} - 1\right)} = L \tag{9}$$

Let $\Delta_f = 1/NT_s$ denote the subcarrier frequency spacing and $f_k = k\Delta_f$ be the normalized frequency of $k-$th subcarrier. We rewrite φ as

$$\varphi = 2\pi T_s\left(k\Delta_f - f\right) = 2\pi T_s\left(f_k - f\right) \tag{10}$$

With (8)—(10), the geometric series can be represented in

$$\sum_{n=-N_{cp}}^{N-1} e^{j2\pi\left(\frac{k}{N} - T_s f\right)n} = L\,\mathrm{s}_L(f - f_k)\, e^{-j\pi T_s (f - f_k)\left(L - 2N_{cp} - 1\right)}, \tag{11}$$

where $\mathrm{s}_L(f)$ is defined as

$$\mathrm{s}_L(f) \cong \begin{cases} (-1)^{T_s f(L-1)}, T_s f \in \mathrm{Z} \\ \dfrac{\sin[\pi L T_s f]}{L \sin[\pi T_s f]}, \text{otherwise} \end{cases} \quad (12)$$

By substituting (11) with (7), we obtain

$$X(f) = \frac{L}{\sqrt{N}} G_I(f) \sum_{k=0}^{N-1} X_k \mathrm{s}_L(f - f_k) e^{-j\pi T_s (f-f_k)(L-2N_{cp}-1)} \quad (13)$$

According to Parseval's theorem [24], the energy of the NC-OFDM signal is given by

$$E_T \cong \int_{-\infty}^{\infty} |x(t)|^2 \, dx = \int_{-\infty}^{\infty} |X(f)|^2 \, df \quad (14)$$

The average power is linearly proportional to the energy, and thus we define the power spectrum density (PSD) as follows

$$S_{XX}(f) \cong \frac{1}{LT_s} |X(f)|^2 = L\Delta_f \left| G_I(f) \sum_{k=0}^{N-1} X_k \mathrm{s}_L(f - f_k) e^{-j\pi T_s (f-f_k)(L-2N_{cp}-1)} \right|^2 \quad (15)$$

Let Φ be the out-of-band interval. The OBP is defined as $\int_{\Phi} S_{XX}(f) \, df$, i.e.,

$$P_{OBP} = \int_{\emptyset} \left| G_I(f) \sum_{k=0}^{N-1} X_k G_N(f) \right|^2 df, \quad (16)$$

However, no analytical expression exists for the integral in (16). In practice, the integral can be estimated based on the Riemann sum [25], and the approximation is as (17).

$$P_{OBP} \cong L\Delta_f \Delta_\beta \sum_{m=1}^{N_\beta} \left| G_I(\beta_m) \sum_{k=0}^{N-1} X_k \mathrm{s}_L(\beta_m - f_k) e^{-j\pi T_s (\beta_m - f_k)(L-2N_{cp}-1)} \right|^2, \quad (17)$$

where β_m denotes the $m-$th frequency sample, Δ_β is the sampling spacing, N_β is the total number of samples laid in the out-of-band interval. For convenience, we express (17) in matrix form as (18).

$$P_{OBP} \cong \left\| \mathbf{A}\vec{\mathrm{X}} \right\|_2^2, \quad (18)$$

where

$$\mathbf{A} = \begin{bmatrix} a_0^0 & a_0^1 & \cdots & a_0^{N-1} \\ a_1^0 & a_1^1 & \cdots & a_1^{N-1} \\ \vdots & \vdots & \ddots & \vdots \\ a_{N_\beta-1}^0 & a_{N_\beta-1}^1 & \cdots & a_{N_\beta-1}^{N-1} \end{bmatrix},$$

and

$$a_m^k = \left(L\Delta_f \Delta_\beta\right)^{\frac{1}{2}} G_I(\beta_m) \mathrm{s}_L(\beta_m - f_k) e^{-j\pi T_s (\beta_m - f_k)(L-2N_{cp}-1)}.$$

C. Peak-to-Average Power Ratio

The discrete-time NC-OFDM signal is generated by $N-$point IFFT; only sample points exist. For the sake of accuracy, we oversample the signal before calculating PAPR. The result after oversampling can be written as

$$x'_n = \frac{1}{\sqrt{N}} \sum_{k=0}^{N-1} X_k e^{j2\pi \frac{k}{QN} n}, n = 0, 1, \ldots, QN-1, \quad (19)$$

where Q is the oversampling factor. From [26] and [27], the estimated PAPR would be accurate enough while $Q \geq 4$. The QN samples in (19) can be represented in vector form as

$$\vec{\mathrm{x}}' = \left[x'_0 \; x'_1 \cdots x'_{QN-1} \right]^{\mathrm{T}} = \mathbf{B}\vec{\mathrm{X}}, \quad (20)$$

where

$$\mathbf{B} = \begin{bmatrix} b_{Q,N}^{0,0} & b_{Q,N}^{0,1} & \cdots & b_{Q,N}^{0,N-1} \\ b_{Q,N}^{1,0} & b_{Q,N}^{1,1} & \cdots & b_{Q,N}^{1,N-1} \\ \vdots & \vdots & \ddots & \vdots \\ b_{Q,N}^{QN-1,0} & b_{Q,N}^{QN-1,1} & \cdots & b_{Q,N}^{QN-1,N-1} \end{bmatrix},$$

and

$$b_{Q,N}^{n,k} = \frac{1}{\sqrt{N}} \sum_{k=0}^{N-1} e^{j2\pi \frac{k}{QN} n}, n = 0, 1, \ldots, QN-1, k = 0, 1, \ldots, N-1.$$

We can derive the peak power and average power by norm operations. The peak power is

$$P_{peak} = \left\| \vec{\mathrm{x}}' \right\|_\infty^2 = \left\| \mathbf{B}\vec{\mathrm{X}} \right\|_\infty^2, \quad (21)$$

where $\| . \|_\infty$ denotes the infinity norm. The average power of the oversampled signal is given by

$$P_{ave} = \mathrm{E}\left\{ \left| x'_n \right|^2 \right\} = \frac{\left\| \mathbf{B}\vec{\mathrm{X}} \right\|_2^2}{QN} \quad (22)$$

where $\mathrm{E}\{ . \}$ is the expectation operation and $\| . \|_2$ denotes the Euclidean norm. With (21) and (22), the PAPR is written as

$$PAPR \cong \frac{\text{Peak Power}}{\text{Average Power}} = \frac{P_{peak}}{P_{ave}} = \frac{QN \left\| \mathbf{B}\vec{\mathrm{X}} \right\|_\infty^2}{\left\| \mathbf{B}\vec{\mathrm{X}} \right\|_2^2} \quad (23)$$

D. Receiver

We consider there are $\mathrm{M_r}$ receive antennas, and the channel impulse response between the transmitter and the $m-$th receive antenna is

$$\vec{\mathrm{h}}_m = \left[h_{m,0} \; h_{m,1} \ldots h_{m,L_c-1} \ldots h_{m,N-1} \right]^{\mathrm{T}}, \quad (24)$$

$\forall k > L_c - 1, h_{m,k} = 0$, L_c is the channel length. The receiver and the first-stage demodulator are shown in **Fig. 2** and **Fig. 3**. By supposing $L_c \leq N_{cp}$, the linear convolution can be replaced with circular convolution while CP is discarded. We define the channel matrix as

$$\mathbf{H}_m = \mathrm{toeplitz}\left(\vec{\mathrm{h}}_m\right) = \begin{bmatrix} h_{m,0} & h_{m,N-1} & h_{m,N-2} & \cdots & h_{m,1} \\ h_{m,1} & h_{m,0} & h_{m,N-1} & \cdots & h_{m,2} \\ h_{m,2} & h_{m,1} & h_{m,0} & \ddots & \vdots \\ \vdots & \vdots & \vdots & \ddots & h_{m,N-1} \\ h_{m,N-1} & h_{m,N-2} & h_{m,N-3} & \cdots & h_{m,0} \end{bmatrix}, \quad (25)$$

and the received signal after removing CP is given by

$$\vec{\mathrm{y}}_m = \vec{\mathrm{x}} \# \vec{\mathrm{h}}_m + \vec{\mathrm{z}}_m = \mathbf{H}_m \vec{\mathrm{x}} + \vec{\mathrm{z}}_m, \quad (26)$$

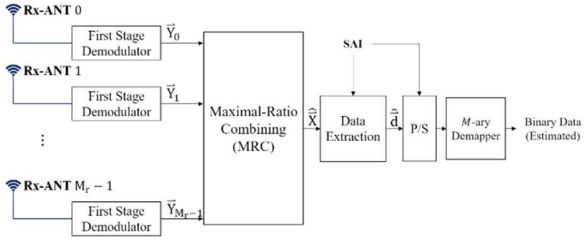

Fig. 2. The NC-OFDM Receiver.

where # denotes circular convolution and $\vec{z}_m$ is an additive Gaussian noise (AWGN) vector. The FFT output of $\vec{y}_m$ is

$$\vec{Y}_m = \mathbf{F}\vec{y}_m = \mathbf{F}\mathbf{H}_m\mathbf{F}^{-1}\vec{X} + \vec{Z}_m, \quad (27)$$

where $\vec{Z}_m = \mathbf{F}\vec{z}_m$. Since the channel matrix is a circulant matrix, the matrix term, $\mathbf{F}\mathbf{H}_m\mathbf{F}^{-1}$, is a diagonal matrix. Let

$$\mathbf{\Lambda}_m = \mathbf{F}\mathbf{H}_m\mathbf{F}^{-1} = \begin{bmatrix} \lambda_{m,0} & & \\ & \ddots & \\ & & \lambda_{m,N-1} \end{bmatrix}, \quad (28)$$

where $\left[\lambda_{m,0}\ \lambda_{m,1}\ \ldots \lambda_{m,N-1}\right]^{\mathrm{T}} = \mathbf{F}\vec{h}_m$ are the eigenvalues of $\mathbf{H}_m$. We rewrite (27) as

$$\vec{Y}_m = \mathbf{\Lambda}_m\vec{X} + \vec{Z}_m \quad (29)$$

Following the first demodulation stage, the maximal-ratio combining (MRC) is adopted to amalgamate the signals corresponding to the $\mathrm{M_r}$ antennas. The first step of MRC is to eliminate the phases caused by the fading channel to maximize the channel gains as follows.

$$\mathbf{\Lambda}_m^{\dagger}\vec{Y}_m = \mathbf{\Lambda}_m^{\dagger}\mathbf{\Lambda}_m\vec{X} + \mathbf{\Lambda}_m^{\dagger}\mathbf{F}\vec{z}_m, \quad (30)$$

where $(.)^{\dagger}$ is the Hermitian transpose operation. Next, combine them into one term as follows.

$$\sum_{m=0}^{\mathrm{M_r}-1}\mathbf{\Lambda}_m^{\dagger}\vec{Y}_m = \sum_{m=0}^{\mathrm{M_r}-1}\left[\mathbf{\Lambda}_m^{\dagger}\mathbf{\Lambda}_m\right]\vec{X} + \sum_{m=0}^{\mathrm{M_r}-1}\left[\mathbf{\Lambda}_m^{\dagger}\vec{Z}_m\right] \quad (31)$$

Lastly, normalize the signal

$$\hat{\vec{X}} = \left\{\sum_{m=0}^{\mathrm{M_r}-1}\left[\mathbf{\Lambda}_m^{\dagger}\mathbf{\Lambda}_m\right]\right\}^{-1}\sum_{m=0}^{\mathrm{M_r}-1}\mathbf{\Lambda}_m^{\dagger}\vec{Y}_m = \vec{X} + \vec{Z}_{MRC}, \quad (32)$$

where $\vec{Z}_{MRC} = \left\{\sum_{m=0}^{\mathrm{M_r}-1}\left[\mathbf{\Lambda}_m^{\dagger}\mathbf{\Lambda}_m\right]\right\}^{-1}\sum_{m=0}^{\mathrm{M_r}-1}\left[\mathbf{\Lambda}_m^{\dagger}\vec{Z}_m\right]$. The signal terms in (30) are multiplied with scales with the same sign, leading to a constructive combination as the former term in (31). In contrast, the noise terms might counteract each other, and the power gain of noise after combining won't be greater than the power gain of the signal. Consequently, MRC could enhance the signal-to-noise ratio (SNR), and the bit error rate (BER) would be improved theoretically.

After MRC, the data symbols of SU can be obtained by data extraction, which requires the SAI. At the transmitter, the data symbols of SU are allocated to a part of the subcarriers. To recover the data of SU, the SAI must be available at the receiver; otherwise, we might extract the wrong data, which can be regarded as interference caused by PU signals or adjusting variables. The issue is "how to acquire the SAI at the receiver". A simple way is to transmit the SAI through a dedicated channel. However, it would cause additional overheads of bandwidth. Another manner is to estimate the SAI, such as the detection scheme presented in [28]. This detection scheme utilizes the received training sequence and channel information to obtain the "a posteriori probability" (APP) of the subcarrier state being occupied or activated by SU. If the APP of $k-$th subcarrier exceeds the decision threshold, the $k-$th subcarrier would be regarded as one of the SU subcarriers.

We suppose the SAI is perfectly estimated using the APP detection scheme and focusing on reducing both OBP and PAPR. We can construct two diagonal matrices with the SAI

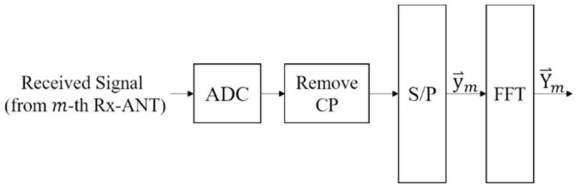

Fig. 3. The First Stage Demodulator.

that can extract PU's and SU's data, respectively. The extraction matrices for SU and PU are given by

$$\text{SU: } \mathbf{I}_{\boldsymbol{D}} = \begin{bmatrix} I_0 & & \\ & \ddots & \\ & & I_{N-1} \end{bmatrix},\ I_k = \begin{cases} 1, k \in \boldsymbol{D} \\ 0, \text{otherwise} \end{cases}; \quad (33)$$

$$\text{PU: } \mathbf{I}_{PU} = \begin{bmatrix} I'_0 & & \\ & \ddots & \\ & & I'_{N-1} \end{bmatrix},\ I'_k = \begin{cases} 1, k \in \boldsymbol{D}_{PU} \\ 0, \text{otherwise} \end{cases} \quad (34)$$

By multiplying $\hat{\vec{X}}$ with $\mathbf{I}_{\boldsymbol{D}}$, we can extract the estimated data vector of SU

$$\hat{\vec{d}} = \mathbf{I}_{\boldsymbol{D}}\hat{\vec{X}} \quad (35)$$

Finally, the binary data could be retrieved by a demapper.

III. The Proposed Optimization Method

Generally speaking, the PAPR and OBP are dependent; if we suppress the OBP, the PAPR would be varied simultaneously, and vice versa. Most of the time, the overall performance would be worsened if we only improved one of the PAPR and OBP. Our method prioritizes OBP reduction or PAPR reduction, depending on the application scenario. The main reason is that the optimization problem might be infeasible if we simultaneously restrict the OBP and PAPR. Therefore, we aim to minimize the minor parameter while the major requirement is satisfied. The OBP and peak power requirements are denoted by ξ_{OBP} and η_{peak}. Let $\vec{X}^{\star}$ be the optimal solution produced by our algorithm. The design criteria we conceived are organized in the following subsection.

A. Design Criteria

1) **The optimal solution must meet the major requirement.**
   If OBP reduction has priority, the OBP of the optimal solution cannot be greater than the OBP requirement. Conversely, the peak power of the optimal solution should obey the peak power constraint, while PAPR reduction is the priority.
2) **The SU subcarriers are reserved.**
   In other words, the data of SU won't be varied by the algorithm. (i.e. $\mathbf{I}_{\boldsymbol{D}}\vec{X}^{\star} = \vec{d}$)
3) **The variables on the PU subcarriers are restricted to prevent the error rate of PU from drastically deteriorating.**
   Precisely, we confine these variables' real and imaginary parts to a square area with sides of length $\nu\rho_{\min}$, which $\rho_{\min}$ denotes the minimum Euclidean distance between

This article has been accepted for publication in IEEE Open Journal of Signal Processing. This is the author's version which has not been fully edited and content may change prior to final publication. Citation information: DOI 10.1109/OJSP.2023.3329757

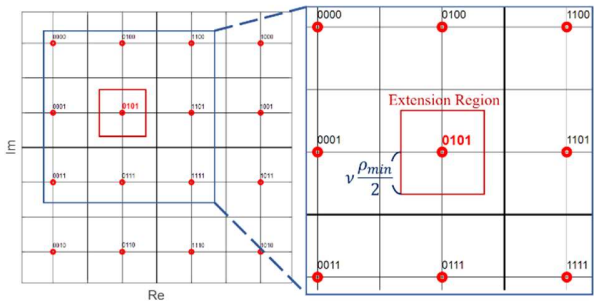

Fig. 4. The Schematic for Criterion 3 with 16QAM Constellation.

two different constellation points and ν is defined as the "extension factor." This criterion can be expressed as

$$\left\|\Re\{I_{PU}\vec{X}^{\prime}\}\right\|_{\infty} \le \nu\frac{\rho_{min}}{2};$$
$$\left\|\Im\{I_{PU}\vec{X}^{\prime}\}\right\|_{\infty} \le \nu\frac{\rho_{min}}{2}, \quad (36)$$

where $\Re\{.\}$ and $\Im\{.\}$ are denote as the real part and the imaginary part, respectively.

For instance, considering 16QAM is adopted, the PU's data symbol 0101 would be extended within the red square in **Fig. 4** as the variable obeying the third criterion has been directly added in. Although the channel effect is ignored here, we can easily find that the variable interferes with PU. If we choose the extension factor appropriately, the BER of PU in the presence of SU could be nearly the same as that in the absence of SU.

With the above criteria, we formulate two algorithms, Algorithm-I and Algorithm-II, corresponding to the two branches in our method.

B. Algorithm-I

Algorithm-I (ALG.I) is for the case where OBP reduction takes priority. It guarantees the OBP follows the requirement, and the peak power with the constraints corresponding to the design criteria could be minimized.

$$\begin{aligned}
&\underset{\vec{X}'}{\text{mimimize}} && \left\|\mathbf{B}\vec{X}'\right\|_{\infty}^{2} \\
&\text{subject to} && \left\|\mathbf{A}\vec{X}'\right\|_{2}^{2} \le \xi_{OBP} \\
&\text{ALG.I:} && \mathbf{I}_{D}\vec{X}' = \vec{d} \\
& && \left\|\Re\left\{\mathbf{I}_{PU}\vec{X}'\right\}\right\|_{\infty} \le \nu\frac{\rho_{\min}}{2} \\
& && \left\|\Im\left\{\mathbf{I}_{PU}\vec{X}'\right\}\right\|_{\infty} \le \nu\frac{\rho_{\min}}{2}
\end{aligned} \quad (37)$$

C. Algorithm-II

In contrast to ALG.I, the second algorithm, Algorithm-II (ALG.II), is prepared for the situation where the PAPR reduction is prior. The objective is to minimize the minor parameter, OBP; meanwhile, the peak power limitation and the constraints are satisfied.

$$\begin{aligned}
&\underset{\vec{X}'}{\text{mimimize}} && \left\|\mathbf{A}\vec{X}'\right\|_{2}^{2} \\
&\text{subject to} && \left\|\mathbf{B}\vec{X}'\right\|_{\infty}^{2} \le \eta_{peak} \\
&\text{ALG.II:} && \mathbf{I}_{D}\vec{X}' = \vec{d} \\
& && \left\|\Re\left\{\mathbf{I}_{PU}\vec{X}'\right\}\right\|_{\infty} \le \nu\frac{\rho_{\min}}{2} \\
& && \left\|\Im\left\{\mathbf{I}_{PU}\vec{X}'\right\}\right\|_{\infty} \le \nu\frac{\rho_{\min}}{2}
\end{aligned} \quad (38)$$

The flowgraph of the optimization method is constructed with ALG.I and ALG.II are described in **Fig. 5**.

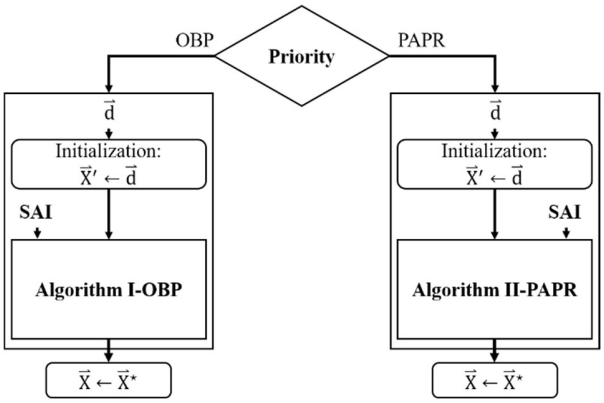

Fig. 5. The Proposed Optimization Method.

D. Convexity Examination

For an optimization problem, convexity is an important indicator since it would determine how to solve this problem via a convex or non-convex approach. According to the definition, an optimization problem is convex if and only if the objective function is convex for minimizing or concave for maximizing, and the feasible region must be convex. The following two tests will examine the convexity of the objective function and feasible region of ALG.I.

In the Appendix, we have proved the objective function and the feasible region of ALG.I are convex. Therefore, we can say ALG.I is a convex optimization problem. In the same way, it can be verified that ALG.II is a convex optimization problem as well. One of the benefits of convex optimization is "the solution is a global minimum," and there are several existing approaches for solving convex optimization, such as the interior-point method (IPM) [29][30].

E. Convexity Examination

In this subsection, we will derive the analytical solutions of ALG.I and ALG.II by using the method of Lagrange multiplier and Karush-Kuhn-Tucker (KKT) conditions.

We first focus on ALG.I merge the constraints to the objective function with Lagrange multipliers.

1) **Lagrangian of ALG.I**

$$\begin{aligned} L(\vec{\mathrm{X}}',\vec{\gamma},\mu_1,\mu_2,\mu_3) &= \left\|\mathbf{B}\vec{\mathrm{X}}'\right\|_\infty^2 + \vec{\gamma}^{\mathrm{T}}\left(\mathbf{I}_{\boldsymbol{D}}\vec{\mathrm{X}}' - \vec{\mathrm{d}}\right) \\ &+\mu_1\left(\left\|\mathbf{A}\vec{\mathrm{X}}'\right\|_2^2 - \xi_{OBP}\right) \\ &+\mu_2\left(\left\|\Re\left\{\mathbf{I}_{PU}\vec{\mathrm{X}}'\right\}\right\|_\infty - \nu\frac{\rho_{\min}}{2}\right) \\ &+\mu_3\left(\left\|\Im\left\{\mathbf{I}_{PU}\vec{\mathrm{X}}'\right\}\right\|_\infty - \nu\frac{\rho_{\min}}{2}\right), \end{aligned} \tag{39}$$

where μ_1,μ_2,μ_3 and the elements of $\vec{\gamma}$ are so-called "Lagrange multipliers". Let $\vec{\mathrm{X}}^{U1}$ be a minimizer of ALG.I, and it must satisfy the Karush-Kuhn-Tucker (KKT) conditions.

2) **KKT conditions**

a) Primal Feasibility

$$\begin{aligned} &\left\|\mathbf{A}\vec{\mathrm{X}}^{U1}\right\|_2^2 - \xi_{OBP} \le 0 \\ &\mathbf{I}_{\boldsymbol{D}}\vec{\mathrm{X}}^{U1} - \vec{\mathrm{d}} = 0 \\ &\left\|\Re\left\{\mathbf{I}_{PU}\vec{\mathrm{X}}^{U1}\right\}\right\|_\infty - \nu\frac{\rho_{\min}}{2} \le 0 \\ &\left\|\Im\left\{\mathbf{I}_{PU}\vec{\mathrm{X}}^{U1}\right\}\right\|_\infty - \nu\frac{\rho_{\min}}{2} \le 0 \end{aligned} \tag{40}$$

b) Dual Feasibility

$$\vec{\gamma} \pm \vec{1}, \mu_1 \ge 0, \mu_2 \ge 0, \mu_3 \ge 0, \tag{41}$$

where $\pm$ is elementwise $\ge$, and $\vec{1}$ is an $N\times 1$ vector whose elements are ones.

c) Complementary Slackness

$$\mu_1\left(\left\|\mathbf{A}\vec{\mathrm{X}}^{U1}\right\|_2^2 - \xi_{OBP}\right) = 0 \tag{42}$$

$$\mu_2\left(\left\|\Re\left\{\mathbf{I}_{PU}\vec{\mathrm{X}}^{U1}\right\}\right\|_\infty - \nu\frac{\rho_{\min}}{2}\right) = 0 \tag{43}$$

$$\mu_3\left(\left\|\Im\left\{\mathbf{I}_{PU}\vec{\mathrm{X}}^{U1}\right\}\right\|_\infty - \nu\frac{\rho_{\min}}{2}\right) = 0 \tag{44}$$

d) Stationarity

$$\nabla_{\vec{\mathrm{X}}} L(\vec{\mathrm{X}}^{U1},\vec{\gamma},\mu_1,\mu_2,\mu_3) = \vec{0}, \tag{45}$$

where ∇ denotes gradient, and $\vec{0}$ is an $N\times 1$ zero vector.

We presume the ℓ_1-th term of $\mathbf{B}\vec{\mathrm{X}}'$, the ℓ_2-term of $\Re\left\{\mathbf{I}_{PU}\vec{\mathrm{X}}'\right\}$, and the ℓ_3- term of $\Im\left\{\mathbf{I}_{PU}\vec{\mathrm{X}}'\right\}$ have the maximal absolute values corresponding to the three infinity norm terms, $\left\|\mathbf{B}\vec{\mathrm{X}}'\right\|_\infty^2$, $\left\|\Re\left\{\mathbf{I}_{PU}\vec{\mathrm{X}}'\right\}\right\|_\infty$, and $\left\|\Im\left\{\mathbf{I}_{PU}\vec{\mathrm{X}}'\right\}\right\|_\infty$.

The gradient of the Lagrangian, (39) is given by

$$\begin{aligned} &\nabla_{\vec{X}'}\mathscr{L}(\vec{X}',\vec{\gamma},\mu_1,\mu_2,\mu_3) \\ &= 2\vec{b}_{\ell_1}^T\vec{b}_{\ell_1}\vec{X}' + I_D\vec{\gamma}^T + 2\mu_1 A^\dagger \quad A\vec{X}' \\ &+\frac{1}{2}\mu_2 I_{PU}\vec{e}_{\ell_2} + \frac{1}{2}\mu_3 I_{PU}\vec{e}_{\ell_3}, \end{aligned} \tag{46}$$

where $\vec{\mathrm{b}}_{\ell_1}$ is the ℓ_1-th row of $\mathbf{B}$, and $\vec{e}_k$ denotes the $k-$th standard basis of N dimension space. With (46), we can solve (45) to obtain $\vec{\mathrm{X}}^{U1}$ as

$$\begin{aligned} \vec{X}^{U1} = -\frac{1}{4}(\vec{b}_{\ell_1}^T\vec{b}_{\ell_1} + \mu_1 A^\dagger \quad A)^{-1}(2I_D\vec{\gamma}^T + \mu_2 I_{PU}\vec{e}_{\ell_2} \\ + \mu_3 I_{PU}\vec{e}_{\ell_3}) \end{aligned} \tag{47}$$

The analytical solution (minimizer) of ALG.I is derived in (47) and the theoretical minimal peak power of ALG.I is

$$\begin{aligned} \left\|\mathbf{B}\vec{\mathrm{X}}^{U1}\right\|_\infty^2 &= \left\|\mathbf{B}\left[-\frac{1}{4}(\vec{\mathrm{b}}_{\ell_1}^{\mathrm{T}}\vec{\mathrm{b}}_{\ell_1} + \mu_1\mathbf{A}^\dagger\mathbf{A})^{-1}(2\mathbf{I}_{\boldsymbol{D}}\vec{\gamma}^{\mathrm{T}} + \mu_2\mathbf{I}_{PU}\vec{e}_{\ell_2} + \mu_3\mathbf{I}_{PU}\vec{e}_{\ell_3})\right]\right\|_\infty^2 \\ &= \frac{1}{16}\left\|\mathbf{B}(\vec{\mathrm{b}}_{\ell_1}^{\mathrm{T}}\vec{\mathrm{b}}_{\ell_1} + \mu_1\mathbf{A}^\dagger\mathbf{A})^{-1}(2\mathbf{I}_{\boldsymbol{D}}\vec{\gamma}^{\mathrm{T}} + \mu_2\mathbf{I}_{PU}\vec{e}_{\ell_2} + \mu_3\mathbf{I}_{PU}\vec{e}_{\ell_3})\right\|_\infty^2 \end{aligned} \tag{48}$$

With similar means, the analytical solution of ALG.II can also be obtained.

3) **Lagrangian of ALG.II**

$$\begin{aligned} L(\vec{\mathrm{X}}',\vec{\kappa},\mu_4,\mu_5,\mu_6) &= \left\|\mathbf{A}\vec{\mathrm{X}}'\right\|_2^2 + \vec{\kappa}^{\mathrm{T}}\left(\mathbf{I}_{\boldsymbol{D}}\vec{\mathrm{X}}' - \vec{\mathrm{d}}\right) \\ &+\mu_4\left(\left\|\mathbf{B}\vec{\mathrm{X}}'\right\|_\infty^2 - \eta_{peak}\right) \\ &+\mu_5\left(\left\|\Re\left\{\mathbf{I}_{PU}\vec{\mathrm{X}}'\right\}\right\|_\infty - \nu\frac{\rho_{\min}}{2}\right) \\ &+\mu_6\left(\left\|\Im\left\{\mathbf{I}_{PU}\vec{\mathrm{X}}'\right\}\right\|_\infty - \nu\frac{\rho_{\min}}{2}\right), \end{aligned} \tag{49}$$

where μ_4,μ_5,μ_6, and the elements of $\vec{\kappa}$ are Lagrange multipliers. Let $\vec{\mathrm{X}}^{U2}$ be a minimizer of ALG.II.

4) **KKT conditions**

a) Primal Feasibility

$$\begin{aligned} &\left\|\mathbf{B}\vec{\mathrm{X}}^{U2}\right\|_\infty^2 - \eta_{peak} \le 0 \\ &\mathbf{I}_{\boldsymbol{D}}\vec{\mathrm{X}}^{U2} - \vec{\mathrm{d}} = 0 \\ &\left\|\Re\left\{\mathbf{I}_{PU}\vec{\mathrm{X}}^{U2}\right\}\right\|_\infty - \nu\frac{\rho_{\min}}{2} \le 0 \\ &\left\|\Im\left\{\mathbf{I}_{PU}\vec{\mathrm{X}}^{U2}\right\}\right\|_\infty - \nu\frac{\rho_{\min}}{2} \le 0 \end{aligned} \tag{50}$$

b) Dual Feasibility

$$\vec{\kappa} \pm \vec{1}, \mu_4 \ge 0, \mu_5 \ge 0, \mu_6 \ge 0 \tag{51}$$

c) Complementary Slackness

$$\mu_4\left(\left\|\mathbf{B}\vec{\mathrm{X}}'\right\|_\infty^2 - \eta_{peak}\right) = 0 \tag{52}$$

$$\mu_5\left(\left\|\Re\left\{\mathbf{I}_{PU}\vec{\mathrm{X}}'\right\}\right\|_\infty - \nu\frac{\rho_{\min}}{2}\right) = 0 \tag{53}$$

$$\mu_6\left(\left\|\Im\left\{\mathbf{I}_{PU}\vec{\mathrm{X}}'\right\}\right\|_\infty - \nu\frac{\rho_{\min}}{2}\right) = 0 \tag{54}$$

d) Complementary Slackness

$$\nabla_{\vec{\mathrm{X}}} L(\vec{\mathrm{X}}^{U2},\vec{\gamma},\mu_4,\mu_5,\mu_6) = \vec{0} \tag{55}$$

The gradient of (49) is given by

$$\begin{aligned} &\nabla_{\vec{X}'}\mathscr{L}(\vec{X}',\vec{\kappa},\mu_1,\mu_2,\mu_3) \\ &= 2A^\dagger \quad A\vec{X}' + I_D\vec{\kappa}^T + 2\mu_4\vec{b}_{\ell_1}^T\vec{b}_{\ell_1}\vec{X}'. \\ &+\frac{1}{2}\mu_5 I_{PU}\vec{e}_{\ell_2} + \frac{1}{2}\mu_6 I_{PU}\vec{e}_{\ell_3}, \end{aligned} \tag{56}$$

Substitute (56) for (55)

$$2\mathbf{A}^{\dagger}\mathbf{A}\vec{\mathrm{X}}^{U2}+\mathbf{I}_{\boldsymbol{D}}\vec{\kappa}^{\mathrm{T}}+2\mu_4\vec{\mathrm{b}}_{\ell_1}^{\mathrm{T}}\vec{\mathrm{b}}_{\ell_1}\vec{\mathrm{X}}^{U2}+\frac{1}{2}\mu_5\mathbf{I}_{PU}\vec{e}_{\ell_2}+\frac{1}{2}\mu_6\mathbf{I}_{PU}\vec{e}_{\ell_3}$$

$$\Rightarrow 2(\mathbf{A}^{\dagger}\mathbf{A}+\mu_4\vec{\mathrm{b}}_{\ell_1}^{\mathrm{T}}\vec{\mathrm{b}}_{\ell_1})\vec{\mathrm{X}}^{U2}=-\frac{1}{2}(2\mathbf{I}_{\boldsymbol{D}}\vec{\kappa}^{\mathrm{T}}+\mu_5\mathbf{I}_{PU}\vec{e}_{\ell_2}+\mu_6\mathbf{I}_{PU}\vec{e}_{\ell} \quad (57)$$

$$\Rightarrow \vec{\mathrm{X}}^{U2}=-\frac{1}{4}(\mathbf{A}^{\dagger}\mathbf{A}+\mu_4\vec{\mathrm{b}}_{\ell_1}^{\mathrm{T}}\vec{\mathrm{b}}_{\ell_1})^{-1}(2\mathbf{I}_{\boldsymbol{D}}\vec{\kappa}^{\mathrm{T}}+\mu_5\mathbf{I}_{PU}\vec{e}_{\ell_2}+\mu_6\mathbf{I}_{PU}\vec{e}_{\ell}$$

The analytical form $\vec{\mathrm{X}}^{U2}$ is given by (57), and the minimal theoretical OBP of ALG.II is

$$\left\|\mathbf{A}\vec{\mathrm{X}}^{U2}\right\|_2^2=\left\|\mathbf{A}\left[-\frac{1}{4}(\mathbf{A}^{\dagger}\mathbf{A}+\mu_4\vec{\mathrm{b}}_{\ell_1}^{\mathrm{T}}\vec{\mathrm{b}}_{\ell_1})^{-1}(2\mathbf{I}_{\boldsymbol{D}}\vec{\kappa}^{\mathrm{T}}+\mu_5\mathbf{I}_{PU}\vec{e}_{\ell_2}+\mu_6\mathbf{I}_{PU}\vec{e}_{\ell_3})\right]\right\|_2^2$$
$$=\frac{1}{16}\left\|\mathbf{A}(\mathbf{A}^{\dagger}\mathbf{A}+\mu_4\vec{\mathrm{b}}_{\ell_1}^{\mathrm{T}}\vec{\mathrm{b}}_{\ell_1})^{-1}(2\mathbf{I}_{\boldsymbol{D}}\vec{\kappa}^{\mathrm{T}}+\mu_5\mathbf{I}_{PU}\vec{e}_{\ell_2}+\mu_6\mathbf{I}_{PU}\vec{e}_{\ell_3})\right\|_2^2 \quad (58)$$

In (42), specifically, $\mu_1\left(\left\|\mathbf{A}\vec{\mathrm{X}}^{U1}\right\|_2^2-\xi_{OBP}\right)=0$ indicates that, at the optimal solution $\vec{\mathrm{X}}^{U1}$, without loss of generality, either $\mu_1=0$ or $\left\|\mathbf{A}\vec{\mathrm{X}}^{U1}\right\|_2^2=\xi_{OBP}$, depends on the inequality constraint in (43) and (44), $\mu_2=0$ or $\left\|\Re\left\{\mathbf{I}_{PU}\vec{\mathrm{X}}^{U1}\right\}\right\|_\infty=\nu\frac{\rho_{\min}}{2}$, $\mu_3=0$ or $\left\|\Im\left\{\mathbf{I}_{PU}\vec{\mathrm{X}}^{U1}\right\}\right\|_\infty=\nu\frac{\rho_{\min}}{2}$. It is the same for the μ_4, $\mu_5=0$, and μ_6 in (52)-(54). The equations for implementing ALG. I and II are summarized in TABLE I.

TABLE I
SUMMARY OF ALG.I AND ALG.II

ALG.I:

$$\underset{\vec{\mathrm{X}}'}{\text{mimimize}}\ \left\|\mathbf{B}\vec{\mathrm{X}}'\right\|_\infty^2 \text{ s. t. } \left\|\mathbf{A}\vec{\mathrm{X}}'\right\|_2^2\le\xi_{OBP},\quad \mathbf{I}_{\boldsymbol{D}}\vec{\mathrm{X}}'=\vec{\mathrm{d}},\left\|\Re\left\{\mathbf{I}_{PU}\vec{\mathrm{X}}'\right\}\right\|_\infty\le\nu\frac{\rho_{\min}}{2},\left\|\Im\left\{\mathbf{I}_{PU}\vec{\mathrm{X}}'\right\}\right\|_\infty\le\nu\frac{\rho_{\min}}{2} \quad (37)$$

1. $$L(\vec{\mathrm{X}}',\vec{\kappa},\mu_4,\mu_5,\mu_6)=\left\|\mathbf{A}\vec{\mathrm{X}}'\right\|_2^2+\vec{\kappa}^{\mathrm{T}}\left(\mathbf{I}_{\boldsymbol{D}}\vec{\mathrm{X}}'-\vec{\mathrm{d}}\right)+\mu_4\left(\left\|\mathbf{B}\vec{\mathrm{X}}'\right\|_\infty^2-\eta_{peak}\right)+\mu_5\left(\left\|\Re\left\{\mathbf{I}_{PU}\vec{\mathrm{X}}'\right\}\right\|_\infty-\nu\frac{\rho_{\min}}{2}\right)+\mu_6\left(\left\|\Im\left\{\mathbf{I}_{PU}\vec{\mathrm{X}}'\right\}\right\|_\infty-\nu\frac{\rho_{\min}}{2}\right), \quad (39)$$

2. $$\left\|\mathbf{A}\vec{\mathrm{X}}^{U1}\right\|_2^2-\xi_{OBP}\le 0,\mathbf{I}_{\boldsymbol{D}}\vec{\mathrm{X}}^{U1}-\vec{\mathrm{d}}=0,\ \left\|\Re\left\{\mathbf{I}_{PU}\vec{\mathrm{X}}^{U1}\right\}\right\|_\infty-\nu\frac{\rho_{\min}}{2}\le 0,\ \left\|\Im\left\{\mathbf{I}_{PU}\vec{\mathrm{X}}^{U1}\right\}\right\|_\infty-\nu\frac{\rho_{\min}}{2}\le 0$$ ……(40)

3. $\vec{\gamma}\pm\vec{1},\mu_1\ge 0,\mu_2\ge 0,\mu_3\ge 0,$ ……..(41)

4. $$\mu_1\left(\left\|\mathbf{A}\vec{\mathrm{X}}^{U1}\right\|_2^2-\xi_{OBP}\right)=0,\quad \mu_2\left(\left\|\Re\left\{\mathbf{I}_{PU}\vec{\mathrm{X}}^{U1}\right\}\right\|_\infty-\nu\frac{\rho_{\min}}{2}\right)=0,\mu_3\left(\left\|\Im\left\{\mathbf{I}_{PU}\vec{\mathrm{X}}^{U1}\right\}\right\|_\infty-\nu\frac{\rho_{\min}}{2}\right)=0$$ ..(42)-(44)

5. $\nabla_{\vec{\mathrm{X}}}L(\vec{\mathrm{X}}^{U1},\vec{\gamma},\mu_1,\mu_2,\mu_3)=\vec{0}$ ……..(45)

6. $$\vec{\mathrm{X}}^{U1}=-\frac{1}{4}(\vec{\mathrm{b}}_{\ell_1}^{\mathrm{T}}\vec{\mathrm{b}}_{\ell_1}+\mu_1\mathbf{A}^{\dagger}\mathbf{A})^{-1}(2\mathbf{I}_{\boldsymbol{D}}\vec{\gamma}^{\mathrm{T}}+\mu_2\mathbf{I}_{PU}\vec{e}_{\ell_2}+\mu_3\mathbf{I}_{PU}\vec{e}_{\ell_3}) \quad (47)$$

7. $$\left\|\mathbf{B}\vec{\mathrm{X}}^{U1}\right\|_\infty^2=\frac{1}{16}\left\|\left[\mathbf{B}(\vec{\mathrm{b}}_{\ell_1}^{\mathrm{T}}\vec{\mathrm{b}}_{\ell_1}+\mu_1\mathbf{A}^{\dagger}\mathbf{A})^{-1}(2\mathbf{I}_{\boldsymbol{D}}\vec{\gamma}^{\mathrm{T}}+\mu_2\mathbf{I}_{PU}\vec{e}_{\ell_2}+\mu_3\mathbf{I}_{PU}\vec{e}_{\ell_3})\right]\right\|_2^2$$ ……(48)

ALG.II:

$$\underset{\vec{\mathrm{X}}'}{\text{mimimize}}\ \left\|\mathbf{A}\vec{\mathrm{X}}'\right\|_\infty^2 \text{ s. t. } \left\|\mathbf{B}\vec{\mathrm{X}}'\right\|_2^2\le\eta_{peak},\quad \mathbf{I}_{\boldsymbol{D}}\vec{\mathrm{X}}'=\vec{\mathrm{d}},\left\|\Re\left\{\mathbf{I}_{PU}\vec{\mathrm{X}}'\right\}\right\|_\infty\le\nu\frac{\rho_{\min}}{2},\left\|\Im\left\{\mathbf{I}_{PU}\vec{\mathrm{X}}'\right\}\right\|_\infty\le\nu\frac{\rho_{\min}}{2} \quad (38)$$

1. $$L(\vec{\mathrm{X}}',\vec{\kappa},\mu_4,\mu_5,\mu_6)=\left\|\mathbf{A}\vec{\mathrm{X}}'\right\|_2^2+\vec{\kappa}^{\mathrm{T}}\left(\mathbf{I}_{\boldsymbol{D}}\vec{\mathrm{X}}'-\vec{\mathrm{d}}\right)+\mu_4\left(\left\|\mathbf{B}\vec{\mathrm{X}}'\right\|_\infty^2-\eta_{peak}\right)+\mu_5\left(\left\|\Re\left\{\mathbf{I}_{PU}\vec{\mathrm{X}}'\right\}\right\|_\infty-\nu\frac{\rho_{\min}}{2}\right)+\mu_6\left(\left\|\Im\left\{\mathbf{I}_{PU}\vec{\mathrm{X}}'\right\}\right\|_\infty-\nu\frac{\rho_{\min}}{2}\right), \quad (49)$$

2. $$\left\|\mathbf{B}\vec{\mathrm{X}}^{U2}\right\|_\infty^2-\eta_{peak}\le 0,\mathbf{I}_{\boldsymbol{D}}\vec{\mathrm{X}}^{U2}-\vec{\mathrm{d}}=0,\ \left\|\Re\left\{\mathbf{I}_{PU}\vec{\mathrm{X}}^{U2}\right\}\right\|_\infty-\nu\frac{\rho_{\min}}{2}\le 0,\left\|\Im\left\{\mathbf{I}_{PU}\vec{\mathrm{X}}^{U2}\right\}\right\|_\infty-\nu\frac{\rho_{\min}}{2}\le 0 \quad (50)$$

3. $\vec{\kappa}\pm\vec{1},\mu_4\ge 0,\mu_5\ge 0,\mu_6\ge 0$ ……(51)

4. $$\mu_4\left(\left\|\mathbf{B}\vec{\mathrm{X}}'\right\|_\infty^2-\eta_{peak}\right)=0,\quad \mu_5\left(\left\|\Re\left\{\mathbf{I}_{PU}\vec{\mathrm{X}}'\right\}\right\|_\infty-\nu\frac{\rho_{\min}}{2}\right)=0,\mu_6\left(\left\|\Im\left\{\mathbf{I}_{PU}\vec{\mathrm{X}}'\right\}\right\|_\infty-\nu\frac{\rho_{\min}}{2}\right)=0$$ …… (52)-(54)

5. $\nabla_{\vec{\mathrm{X}}}L(\vec{\mathrm{X}}^{U2},\vec{\gamma},\mu_4,\mu_5,\mu_6)=\vec{0}$ ……..(55)

6. $$\vec{\mathrm{X}}^{U2}=-\frac{1}{4}(\mathbf{A}^{\dagger}\mathbf{A}+\mu_4\vec{\mathrm{b}}_{\ell_1}^{\mathrm{T}}\vec{\mathrm{b}}_{\ell_1})^{-1}(2\mathbf{I}_{\boldsymbol{D}}\vec{\kappa}^{\mathrm{T}}+\mu_5\mathbf{I}_{PU}\vec{e}_{\ell_2}+\mu_6\mathbf{I}_{PU}\vec{e}_{\ell_3})$$ ……(57)

7. $$\left\|\mathbf{A}\vec{\mathrm{X}}^{U2}\right\|_2^2=\frac{1}{16}\left\|\mathbf{A}(\mathbf{A}^{\dagger}\mathbf{A}+\mu_4\vec{\mathrm{b}}_{\ell_1}^{\mathrm{T}}\vec{\mathrm{b}}_{\ell_1})^{-1}(2\mathbf{I}_{\boldsymbol{D}}\vec{\kappa}^{\mathrm{T}}+\mu_5\mathbf{I}_{PU}\vec{e}_{\ell_2}+\mu_6\mathbf{I}_{PU}\vec{e}_{\ell_3})\right\|_2^2$$ ……(58)

F. Computational Complexity

For ALG.I and ALG.II, calculating the peak power and OBP would take $QN\times N$ $N_\beta\times N$ complex multiplications. In addition, if we leverage IPM to handle the convex optimization, the complexity is equivalent to N^3 complex multiplications[29][30]. As a result, the overall computational complexity of the method is $O\left(N^3+N_\beta N+QN\right)$. The computational complexity comparisons for the proposed method, POCS[22], and APOCNCS[23] are listed in TABLE II.

TABLE II
COMPUTATIONAL COMPLEXITY COMPARISONS

Methods	Complexity
POCS	$O\left(N_w^3+N^3+QN\times\log(QN)\right)$
APOCNCS	$O\left(2N_w^3+N^3+QN\times\log(QN)\right)$
Proposed Method	$O\left(N^3+N_\beta N+QN\right)$

IV. SIMULATION RESULTS

In the simulation, a total of 64 subcarriers with indices {0, 1, …, 63} are sited in the licensed spectrum. The subcarriers, {16, …, 23, 40, …, 47}, are currently occupied by PU, and we assigned the subcarriers, {1, 4, 6,…, 9, 11, …, 14, 25, …, 28, 30, …, 33, 35, …, 38, 49, …, 52, 54, …, 57, 59, …, 62}, to SU for data transmission. On the transmit side, we employ the solid-state power amplifier (SSPA) [31], which is commonly

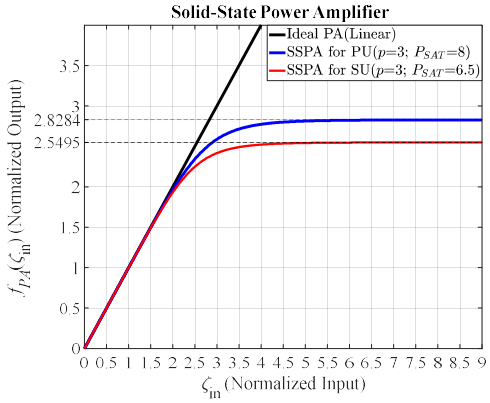

Fig. 6. Characteristic Graph of PA.

used in wireless communication systems due to its high efficiency, high reliability, and long lifespan. The amplitude of SSPA output can be described by

$$f_{PA}(\zeta_{\text{in}}) = \frac{\zeta_{\text{in}}}{\left(1+\left(\frac{\zeta_{\text{in}}}{\sqrt{P_{SAT}}}\right)^{2p}\right)^{\frac{1}{2p}}}, \tag{59}$$

where ζ_{in} is the amplitude of the input signal, p is the sharpness factor, and P_{SAT} denotes the normalized saturation power. We set $p=3$ and $P_{SAT}=8$ for the SSPA adopted by PU's transmitter while the SSPA with $p=3$ and $P_{SAT}=6.5$ is employed by SU. The characteristic curves of an ideal PA and the SSPAs of PU and SU are shown in **Fig. 6**.

There are two kinds of configurations, $\mathrm{M_r}=4$ and $\mathrm{M_r}=16$, at the receiving terminal, the channel in our environment is TDL-B specified by 3GPP [32]. The TDL-B model emulates the non-line-of-sight (NLOS) propagation across frequency bands ranging from 0.5 to 100 GHz. We simulate the UMi Street-canyon scenario with a normal delay profile over the 28 GHz band by extending the TDL-B model according to the scenario-specific scaling factors tabulated in [32] to assess the practical performance. The detailed setup is listed in TABLE III.

To analyze the reduction gains, we define the OBP ratio (OBPR) and the complementary cumulative distribution functions (CCDFs) of PAPR and OBPR [22] as follows

$$\text{OBPR} \cong \frac{\text{out-of-band power}}{\text{total power}} \tag{60}$$

$$\text{CCDF}\{\text{PAPR}\} \cong \Pr\left(\text{PAPR} > \text{PAPR}_0\right) \tag{61}$$

$$\text{CCDF}\{\text{OBPR}\} \cong \Pr\left(\text{OBPR} > \text{OBPR}_0\right) \tag{62}$$

where Pr(.) denotes the probability, PAPR_0 and OBPR_0 are the thresholds of PAPR and OBPR.

Herein, we compare our method with POCS [22] and APOCNCS [23] in OBPR, PAPR, and BER. At first, we consider the situation that OBP reduction with the OBP requirement, $\xi_{OBP}=5$ dB, has priority. To operate POCS and APOCNCS, two parameters are set as $\eta_{peak}=20.5$ dB; $\xi_{IBP}=35.5$ dB. in **Fig. 7** the PAPR reduction gains of POCS and APOCNCS are nearly zero at CCDF 10^{-3}. Meanwhile, ALG.I with $\nu=0.1$ and ALG.I with $\nu=0.3$ still reduce about 2dB of PAPR at CCDF 10^{-3}, and the small gap between the two cases ν is owed to the larger ν one has more freedom to obtain better reduction performance at the expense of slightly increasing the interference to PU. In addition to PAPR and OBPR reduction gains, the BER performances are important, especially the BER of PU.

However, as portrayed In **Fig. 8** we can find that APOCNCS, POCS, and ALG.I with $\nu=0.1, 0.3$ achieve at least 12 dB reduction of OBPR at CCDF 10^{-2}, and APOCNCS has the best OBPR performance, where "Origin" denotes the curve obtained from original NC-OFDM signals without any preprocessing.

TABLE III
SIMULATION PARAMETERS

✓	mapper	QPSK, 4 QAM, 256 QAM, 512 QAM
✓	total number of subcarriers	$N=64,512$
✓	CP length	$N_{cp}=16$
✓	number of out-of-band samples	$N_{\beta}=256$
✓	oversampling factor	$Q=4,5,6,8$,
✓	power amplifier	Solid State Power Amplifier (SSPA)
✓	sharpness factor	$p=3$ for PU and SU
✓	normalized saturation power	$P_{SAT}=8$ for PU; $P_{SAT}=6.5$ for SU
✓	channel model	TDL-B
✓	center frequency	28 GHz
✓	subcarrier spacing	$\Delta_f=60$ kHz
✓	scenario	UMi-Street-canyon
✓	delay spread	66 ns
✓	peak power requirement	$\eta_{peak}=22.5$ dB
✓	OBP requirement	$\xi_{OBP}=5$ dB
✓	extension factor	$\nu=0.1, 0.3$

As shown in **Fig. 9** and **Fig. 10**, our methods outperform POCS and APOCNCS and significantly improve the BER of SU. Specifically, the original SU signals and the SU signals with POCS and APOCNCS suffer from severe intermodulation distortions while passing through PA; hence the error floors occur at signal-to-noise ratio (SNR) dB regardless of the configuration of antennas. Worse still, the results in **Fig. 11** and **Fig. 12** show that the SU signals processed by POCS and APOCNCS cause strong interference to PU and drastically degrade the BER of PU. In contrast, ALG.I with $\nu=0.1,0.3$ not only can improve the BER of SU lower than 10^{-4} at SNR $=20$ dB with 4 receive antennas and at SNR $=10$ dB with 16 receive antennas but also maintain the transmission quality of PU, see **Fig. 9** to **Fig. 12**.

Turning to the next part, PAPR reduction is priority, and the peak power constraint is set as $\eta_{peak}=22.5$ dB. The minor parameters for POCS and APOCNCS are $\xi_{OBP}=5$ dB and $\xi_{IBP}=35.5$ dB. As depicted in **Fig. 13**, both ALG.II with $\nu=0.1$ and ALG.II with $\nu=0.3$ have 1.5 dB reduction of PAPR at CCDF $=10^{-3}$ and prevail over POCS. In **Fig. 14**, it is obvious that POCS and APOCNCS cannot improve the OBPR,

and they even have higher OBPR compared with the original one at CCDF $=10^{-3}$ while the OBPR curves of ALG.II are at least not greater than the original one. On the other hand, the BER results of SU are exhibited in **Fig. 15** and **Fig. 16**. At BER $=10^{-4}$, our method can perform 10 dB improvement with 4 receive antennas and 16 receive antennas. Although the BER results of SU with POCS and APOCNCS is comparable to that with our method, the SU signals with POCS and APOCNCS would introduce considerable interference to PU and result in extremely low transmission quality of PU, see **Fig. 17** and **Fig. 18** Notably, the BER curves of PU in the presence of ALG.II-aided SU are almost the same as that in the absence of SU, that is, the BER of PU won't be degraded by SU with our method.

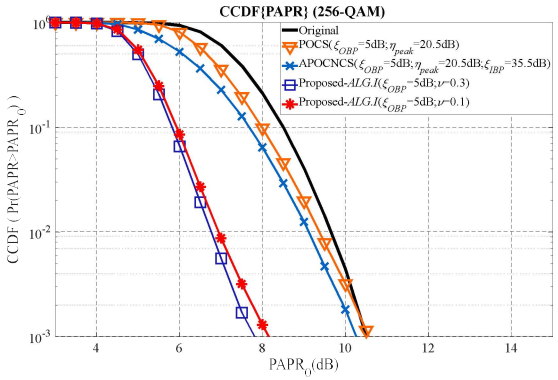

Fig. 7. CCDF of PAPR (OBP reduction takes priority).

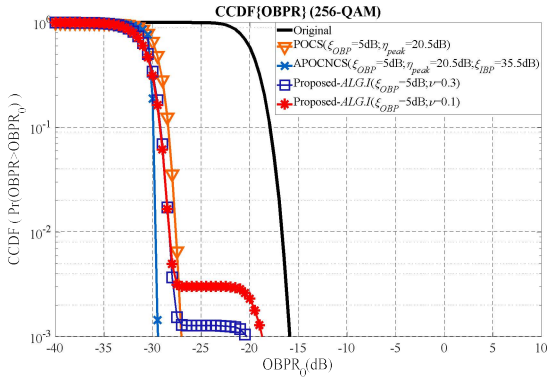

Fig. 8. CCDF for OBPR (OBP reduction takes priority).

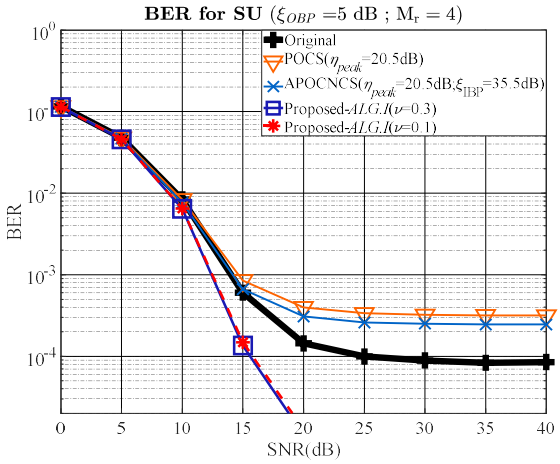

Fig. 9. BER for SU with 4 receive antennas (OBP reduction takes priority).

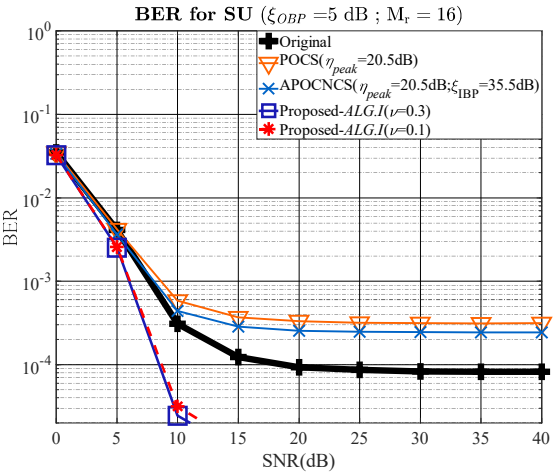

Fig. 10. BER for SU with 16 receive antennas (OBP reduction takes priority).

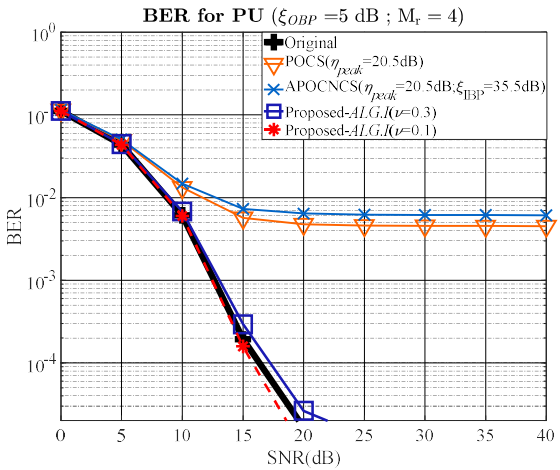

Fig. 11. BER for PU with 4 receive antennas (OBP reduction takes priority).

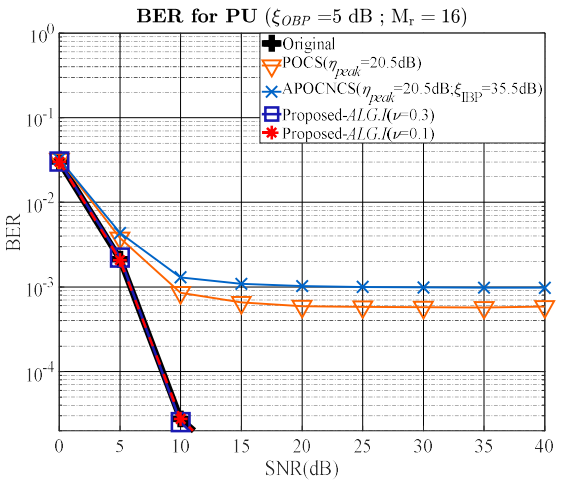

Fig. 12. BER for PU with 16 receive antennas (OBP reduction takes priority).

This article has been accepted for publication in IEEE Open Journal of Signal Processing. This is the author's version which has not been fully edited and content may change prior to final publication. Citation information: DOI 10.1109/OJSP.2023.3329757

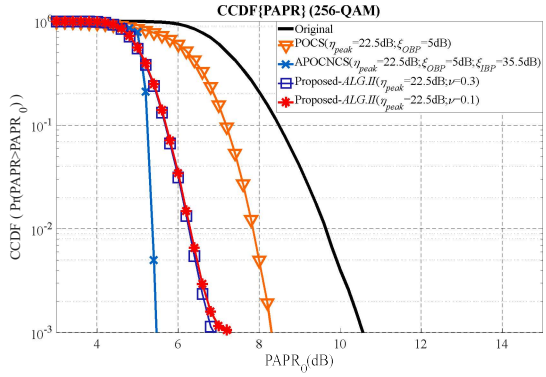

Fig. 13. CCDF for PAPR (PAPR reduction is priority).

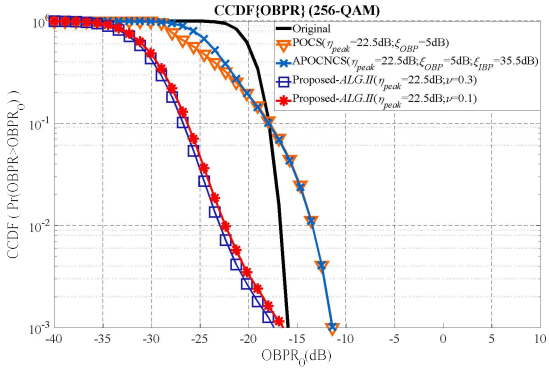

Fig. 14. CCDF for OBPR (PAPR reduction is priority).

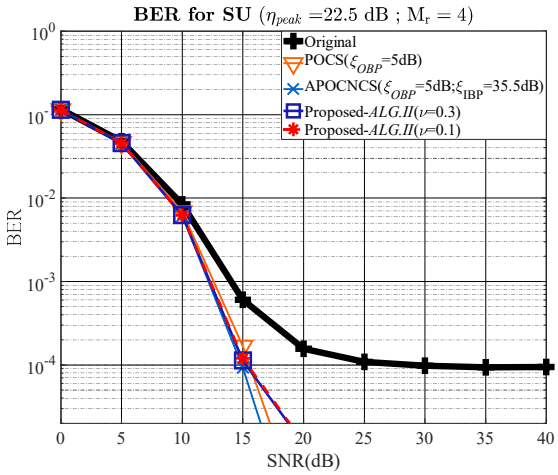

Fig. 15. BER for SU with 4 receive antennas (PAPR reduction is priority)

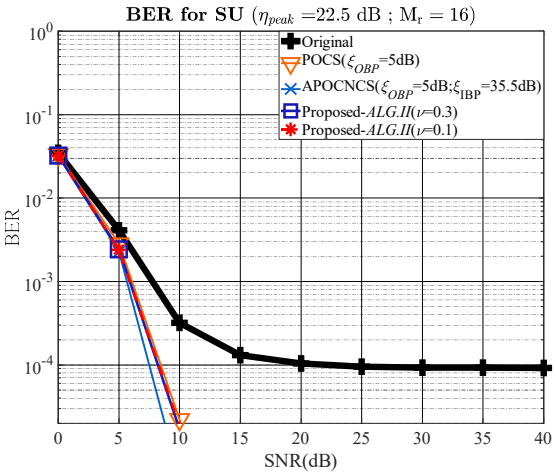

Fig. 16. BER for SU with 16 receive antennas (PAPR reduction is priority).

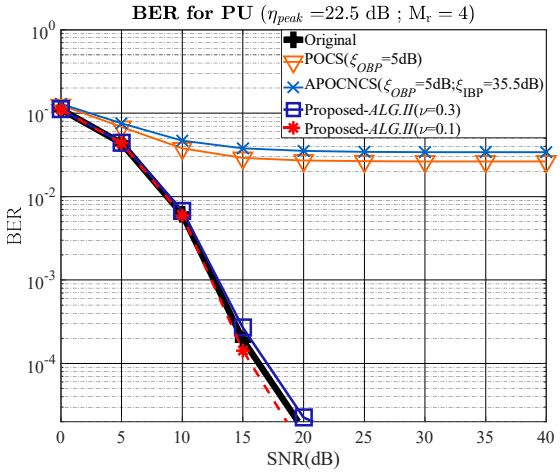

Fig. 17. BER for PU with 4 receive antennas (PAPR reduction is priority).

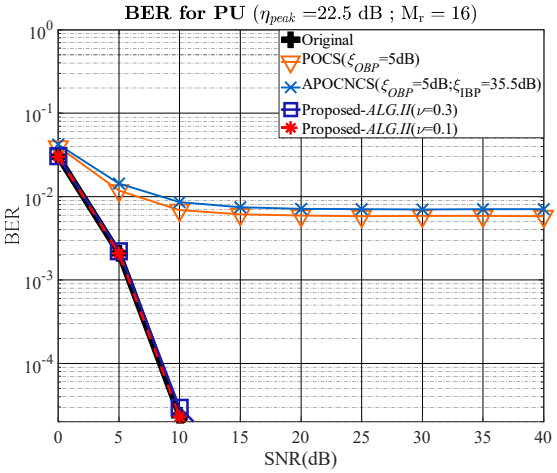

Fig. 18. BER for PU with 16 receive antennas (PAPR reduction is priority).

In **Fig. 19**, we can find that the POCS, and ALG.I with $\nu = 0.1$ achieve 1.02 and 4.08dB reduction of PAPR at CCDF $= 10^{-2}$, respectively. In **Fig. 20**, we can find that the POCS, and ALG.I with $\nu = 0.1$ achieve 5.9 and 6.44dB reduction of OBPR at CCDF $= 10^{-2}$, respectively.

Overall, POCS and APOCNCS can reduce the major parameter, however, the performance of the minor parameter cannot be enhanced and might be exacerbated. Moreover, the NC-OFDM signals of SU with POCS and APOCNCS "dramatically disturb PU", which is strictly forbidden and runs counter to the purpose of using NC-OFDM. The main reason why POCS and APOCNCS introduce high interference to PU is that the power of their weights on the

PU subcarriers is unrestricted. By comparison, we impose the third criterion, the constraint that limits the adjusting variables on PU subcarriers with the extension factor ν , on the proposed optimization algorithms. The simulation results show that the extension factor in our method can effectively prevent SU from interfering with PU, which is favorable and could benefit the collaboration between PU and SU.

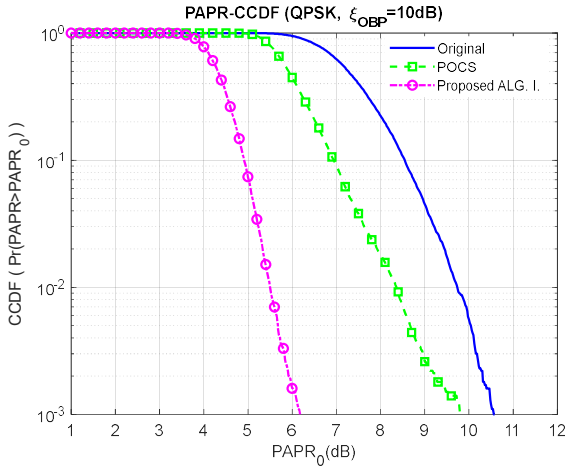

Fig. 19. CCDF for PAPR (OBP reduction takes priority)

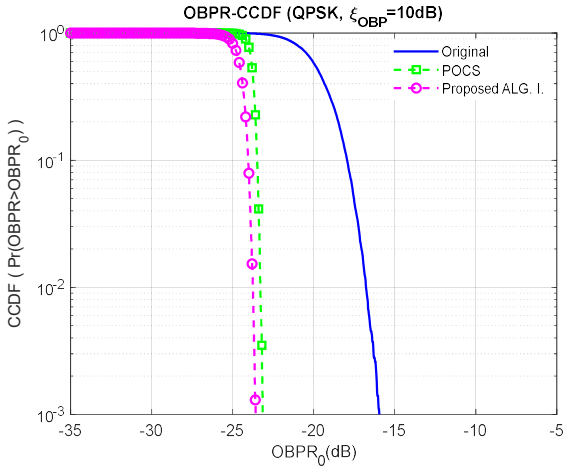

Fig. 20. CCDF for OBPR (OBP reduction takes priority).

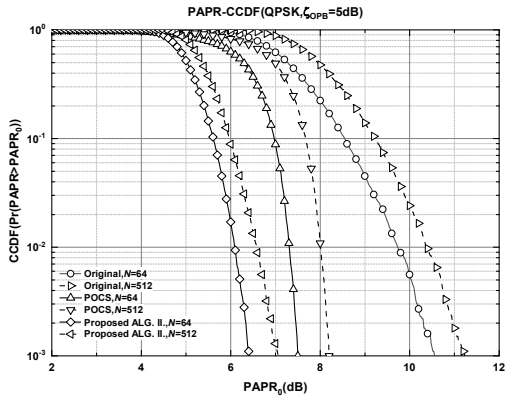

Fig. 21. CCDF for PAPR of the NC-OFDM with different subcarriers (PAPR reduction takes priority).

Fig. 22 shows the distribution of the PAPR of the NC-OFDM signal with Q=4 with different subcarriers. As depicted in **Fig. 22**, the proposed ALG.II with $\nu = 0.1$ is outperforms the POCS as the number of subcarriers increases. It is also observed that the PAPR increases as the number of subcarriers. t The simulation results are similar to the outcomes in the literature [33], [34], and[35], i.e., the smaller subcarriers, the smaller PAPR.

Fig. 22 shows the distribution of the PAPR of the NC-OFDM signal with Q=4 with different modulation orders. As depicted in Fig. 22, the proposed ALG.II with $\nu = 0.1$ is outperforms the POCS as modulation order increases. It is also observed that the PAPR increases with the number of modulation orders. The simulation results are similar to the outcomes in the literature [36] and [37].

Fig. 23 shows the distribution of the PAPR of the NC-OFDM signal with N=64, and Q=4,5,6,8. The PAPR does not increase significantly. This result is similar to the outcomes in the literature [27] and [34]. The OFDM signal is generated using the IFFT at the Nyquist rate. The peak value of the resulting discrete-time OFDM signal samples calculated utilizing the IFFT may not coincide with the peak value of the continuous-time OFDM signal [33]. Hence, an oversampling factor greater than 1 is usually adopted to increase the accuracy, and a commonly adopted oversampling factor is 4 [38][39]. The literature [26] found that if the oversampling factor is at least 4, the difference between the continuous-time and discrete-time PAR is negligible, i.e., the PAPR of the over-sampled discrete-time signal offers an accurate approximation of the PAPR of the continuous-time OFDM signal. The reference [27] has generalized Tellambura's results [26] to complex-valued modulations that the discrete-time PAPR obtained from four-time oversampled signals may be considered a sufficiently accurate approximation of the continuous-time PAPR. Literature [40], [41], and [42] discuss details of the relationship between the oversampled OFDM signal's PAPR and the continuous signal's PAPR. The oversampling rate from 1 to 8, and 1 to 20 are illustrated in [27] and [38], respectively.

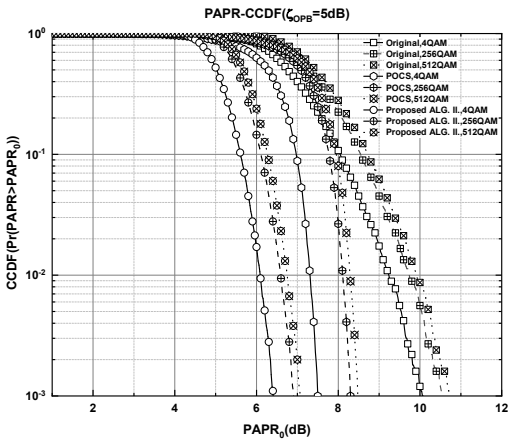

Fig. 22. CCDF for PAPR of the NC-OFDM signal samples with different modulation orders (PAPR reduction takes priority).

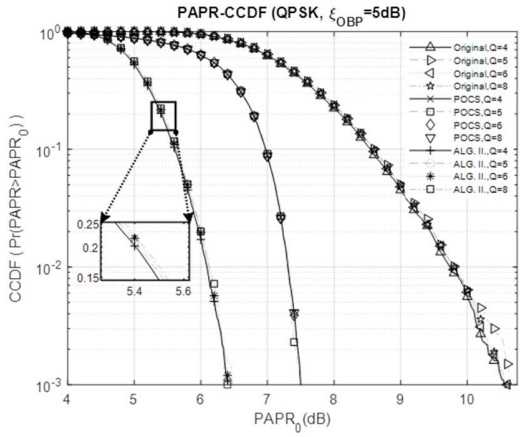

Fig. 23. CCDF for PAPR of the NC-OFDM signal samples oversampled by different Q (PAPR reduction takes priority).

V. Conclusion

This study presents an optimization method to mitigate the PAPR and OBP in the NC-OFDM system. At the same time, OBP reduction is the priority, ALG. I can achieve the OBP requirement and significantly reduce the PAPR. Furthermore, we take PU into account and inspect the BER performance. The published methods, POCS and APOCNCS, only focus on PAPR and OBP, and the BER of PU is omitted. Predictably, the simulation results demonstrate that POCS and APOCNCS would degrade the BER of PU. In comparison, the interference introduced by SU's NC-OFDM signals with our method is small enough to be ignored, and the BER of PU is almost unchanged. The key finding in this research is that if the adjusting variables or weights accommodated by PU subcarriers are meticulously confined, the interference to PU could be controlled. To a secondary user, the main mission is to avoid interfering with primary users regardless of the performance of the secondary system. By using NC-OFDM with our method, it is possible to transmit the data of SU without impacting the BER of PU, which could facilitate the implementation of DSS for future communications. For the prospective study, the spectral mask [43] may be considered as the OBP constraint in the proposed algorithm I. The clipping and filtering methods [44] can eliminate the out-of-band frequency components to minimize OBP in the proposed algorithm II. In Design Criterion 3, the error vector magnitude (EVM) [45] may be considered as the side length of the square.

Appendix

The proof of Test 1(the objective function) and Test 2 (the feasible region) of ALG.I are convex as follows.

1) **Test 1. Objective Function**

a) Definition:

f is a convex function $\Leftrightarrow$ $f\left(\theta\vec{u}_1+(1-\theta)\vec{u}_2\right)\le\theta f(\vec{u}_1)+(1-\theta)f$

where $\theta\in[0,1]$

For instance, the function in **Fig. 24**is convex, and the other one in **Fig. 25** is non-convex. Let

$$f(\vec{X}')=\left\|\mathbf{B}\vec{X}'\right\|_\infty^2,\ \theta\in[0,1]$$

The derivation is as follows

$$\begin{aligned}
&f(\theta\vec{u}_1+(1-\theta)\vec{u}_2)\\
&=\|\theta\mathbf{B}\vec{u}_1+(1-\theta)\theta\vec{u}_2\|_\infty^2\\
&\le[\|\theta\mathbf{B}\vec{u}_1\|_\infty+\|(1-\theta)\mathbf{B}\vec{u}_2\|_\infty]^2\\
&=[\theta\|\mathbf{B}\vec{u}_1\|_\infty+\|(1-\theta)\mathbf{B}\vec{u}_2\|_\infty]^2\\
&=-\theta(1-\theta)[\|\mathbf{B}\vec{u}_1\|_\infty-\|\mathbf{B}\vec{u}_2\|_\infty]^2\\
&\qquad+[\theta\|\mathbf{B}\vec{u}_1\|_\infty^2+(1-\theta)\|\mathbf{B}\vec{u}_2\|_\infty^2]\\
&\le[\theta\|\mathbf{B}\vec{u}_1\|_\infty^2+(1-\theta)\|\mathbf{B}\vec{u}_2\|_\infty^2]\\
&=\theta f(\vec{u}_1)+(1-\theta)f(\vec{u}_2).\\
&\Rightarrow f\left(\theta\vec{u}_1+(1-\theta)\vec{u}_2\right)\le\theta f(\vec{u}_1)+(1-\theta)f(\vec{u}_2),\ \theta\in[0,1]\quad(63)
\end{aligned}$$

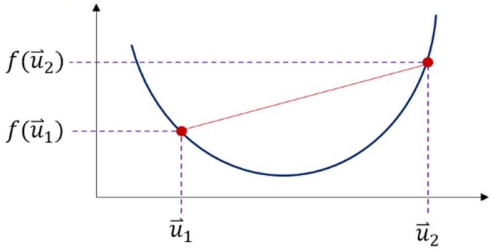

Fig. 24. Convex Function.

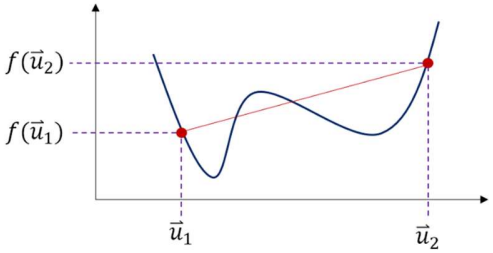

Fig. 25. Non-convex Function.

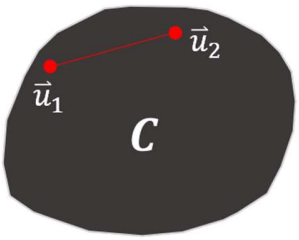

Fig. 26. Convex Set.

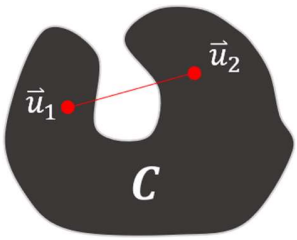

Fig. 27. Non-convex Set

2) **Test2. Feasible Region**

a) Definition:

$\boldsymbol{C}$ is a convex set $\Leftrightarrow$ $\forall\vec{u}_1,\vec{u}_2\in\boldsymbol{C},\left[\theta\vec{u}_1+(1-\theta)\vec{u}_2\right]\in\boldsymbol{C},\ \theta\in[0,1]$

To clarify, a typical convex set and a non-convex set are shown in **Fig. 26** and **Fig. 27**. Let

$$\boldsymbol{C}=\left\{\vec{\mathrm{X}}' \;\middle|\; \left\|\mathbf{A}\vec{\mathrm{X}}'\right\|_2^2 \le \xi_{OBP}, \mathbf{I}_{\boldsymbol{D}}\vec{\mathrm{X}}'=\vec{\mathrm{d}}, \left\|\Re\left\{\mathbf{I}_{PU}\vec{\mathrm{X}}'\right\}\right\|_\infty \le \nu\frac{\rho_{\min}}{2}, \left\|\Im\left\{\mathbf{I}_{PU}\vec{\mathrm{X}}'\right\}\right\|_\infty \le \nu\frac{\rho_{\min}}{2}\right\}$$

where , $\vec{u}_1, \vec{u}_2 \in \boldsymbol{C}, \theta \in [0,1]$.

The proof is given by

$$\begin{aligned}
&\|\mathbf{A}[\theta\vec{u}_1+(1-\theta)\theta\vec{u}_2]\|_2^2 \\
&=\|[\theta\mathbf{A}\vec{u}_1+(1-\theta)\theta\mathbf{A}\vec{u}_2]\|_2^2 \\
&\le [\|[\theta\boldsymbol{A}\vec{u}_1]\|_2+\|(1-\theta)\theta\boldsymbol{A}\vec{u}_2\|_2]^2 \\
&=[\|[\theta\boldsymbol{A}\vec{u}_1]\|_2+\|(1-\theta)\theta\boldsymbol{A}\vec{u}_2\|_2]^2 \\
&\le \left[\theta\sqrt{\xi_{OBP}}+(1-\theta)\sqrt{\xi_{OBP}}\right]^2 \\
&=\left(\sqrt{\xi_{OBP}}\right)^2=\xi_{OBP}.
\end{aligned} \tag{64}$$

$$\mathbf{I}_{\boldsymbol{D}}\left[\theta\vec{u}_1+(1-\theta)\vec{u}_2\right]=\theta\,\mathbf{I}_{\boldsymbol{D}}\vec{u}_1+(1-\theta)\mathbf{I}_{\boldsymbol{D}}\vec{u}_2=\theta\vec{\mathrm{d}}+(1-\theta)\vec{\mathrm{d}}=\vec{\mathrm{d}}$$

$$\Rightarrow \mathbf{I}_{\boldsymbol{D}}\left[\theta\vec{u}_1+(1-\theta)\vec{u}_2\right]=\vec{\mathrm{d}} \tag{65}$$

$$\begin{aligned}
&\left\|\Re\left\{\mathbf{I}_{PU}\left[\theta\vec{u}_1+(1-\theta)\vec{u}_2\right]\right\}\right\|_\infty \\
&=\left\|\theta\,\Re\left\{\mathbf{I}_{PU}\vec{u}_1\right\}+(1-\theta)\Re\left\{\mathbf{I}_{PU}\vec{u}_2\right\}\right\|_\infty \\
&\le \theta\left\|\Re\left\{\mathbf{I}_{PU}\vec{u}_1\right\}\right\|_\infty+(1-\theta)\left\|\Re\left\{\mathbf{I}_{PU}\vec{u}_2\right\}\right\|_\infty \\
&\le \theta\nu\frac{\rho_{\min}}{2}+(1-\theta)\nu\frac{\rho_{\min}}{2}=\nu\frac{\rho_{\min}}{2} \\
&\Rightarrow \left\|\Re\left\{\mathbf{I}_{PU}\left[\theta\vec{u}_1+(1-\theta)\vec{u}_2\right]\right\}\right\|_\infty \le \nu\frac{\rho_{\min}}{2}
\end{aligned} \tag{66}$$

$$\begin{aligned}
&\left\|\Im\left\{\mathbf{I}_{PU}\left[\theta\vec{u}_1+(1-\theta)\vec{u}_2\right]\right\}\right\|_\infty \\
&=\left\|\theta\,\Im\left\{\mathbf{I}_{PU}\vec{u}_1\right\}+(1-\theta)\Im\left\{\mathbf{I}_{PU}\vec{u}_2\right\}\right\|_\infty \\
&\le \theta\left\|\Im\left\{\mathbf{I}_{PU}\vec{u}_1\right\}\right\|_\infty+(1-\theta)\left\|\Im\left\{\mathbf{I}_{PU}\vec{u}_2\right\}\right\|_\infty \\
&\le \theta\nu\frac{\rho_{\min}}{2}+(1-\theta)\nu\frac{\rho_{\min}}{2} \\
&=\nu\frac{\rho_{\min}}{2} \\
&\Rightarrow \left\|\Im\left\{\mathbf{I}_{PU}\left[\theta\vec{u}_1+(1-\theta)\vec{u}_2\right]\right\}\right\|_\infty \le \nu\frac{\rho_{\min}}{2}
\end{aligned} \tag{67}$$

With (64)-(67), we have

$$\begin{aligned}
&\left[\theta\vec{u}_1+(1-\theta)\vec{u}_2\right]\in\boldsymbol{C} \\
&\Rightarrow \forall\vec{u}_1,\vec{u}_2\in\boldsymbol{C},\left[\theta\vec{u}_1+(1-\theta)\vec{u}_2\right]\in\boldsymbol{C},\ \theta\in[0,1],
\end{aligned} \tag{68}$$

And the feasible region is convex.

REFERENCES

[1] M. Parvini *et al*., "Spectrum Sharing Schemes From 4G to 5G and Beyond: Protocol Flow, Regulation, Ecosystem, Economic," in *IEEE Open Journal of the Communications Society*, vol. 4, pp. 464-517, 2023, doi: 10.1109/OJCOMS.2023.3238569.

[2] H. Tataria, M. Shafi, A. F. Molisch, M. Dohler, H. Sjöland and F. Tufvesson, "6G Wireless Systems: Vision, Requirements, Challenges, Insights, and Opportunities," in *Proceedings of the IEEE*, vol. 109, no. 7, pp. 1166-1199, July 2021, doi: 10.1109/JPROC.2021.3061701.

[3] J. Mitola and G. Q. Maguire, "Cognitive radio: making software radios more personal," in IEEE Personal Communications, vol. 6, no. 4, pp. 13-18, Aug. 1999, doi: 10.1109/98.788210.

[4] Y. Liang, K. Chen, G. Y. Li and P. Mahonen, "Cognitive radio networking and communications: an overview," in IEEE Transactions on Vehicular Technology, vol. 60, no. 7, pp. 3386-3407, Sept. 2011, doi: 10.1109/TVT.2011.2158673.

[5] W. S. H. M. W. Ahmad *et al*., "5G Technology: Towards Dynamic Spectrum Sharing Using Cognitive Radio Networks," in *IEEE Access*, vol. 8, pp. 14460-14488, 2020, doi: 10.1109/ACCESS.2020.2966271.

[6] M. Shafi *et al*., "5G: A Tutorial Overview of Standards, Trials, Challenges, Deployment, and Practice," in *IEEE Journal on Selected Areas in Communications*, vol. 35, no. 6, pp. 1201-1221, June 2017, doi: 10.1109/JSAC.2017.2692307.

[7] C. B. Ali Wael, N. Armi, T. Miftahushudur, Y. S. Amrullah and R. Sariningrum, "NC-OFDM Transceiver Design for Maritime Cognitive Radio," *2018 International Conference on Radar, Antenna, Microwave, Electronics, and Telecommunications (ICRAMET)*, Serpong, Indonesia, 2018, pp. 117-120, doi: 10.1109/ICRAMET.2018.8683927.

[8] Bogucka, H., Kliks, A. and Kryszkiewicz, P. (2017). Noncontiguous OFDM for Future Radio Communications. In Advanced Multicarrier Technologies for Future Radio Communication (eds H. Bogucka, A. Kliks and P.Kryszkiewicz). doi:10.1002/9781119168935.ch3.

[9] D. Serghiou, M. Khalily, T. W. C. Brown and R. Tafazolli, "Terahertz Channel Propagation Phenomena, Measurement Techniques and Modeling for 6G Wireless Communication Applications: A Survey, Open Challenges and Future Research Directions," in *IEEE Communications Surveys & Tutorials*, vol. 24, no. 4, pp. 1957-1996, Fourthquarter 2022, doi: 10.1109/COMST.2022.3205505.

[10] P. Wei, L. Dan, C. Zhou, Y. Xiao, G. Wu and S. Li, "Joint optimization of peak-to-average power ratio and spectral leakage in 5G multicarrier waveforms," in *China Communications*, vol. 12, no. Supplement, pp. 83-92, December 2015, doi: 10.1109/CC.2015.7386156.

[11] Ai Bo, Yang Zhi-xing, Pan Chang-yong, Zhang Tao-tao and Ge Jian-hua, "Effects of PAPR reduction on HPA predistortion," in *IEEE Transactions on Consumer Electronics*, vol. 51, no. 4, pp. 1143-1147, Nov. 2005, doi: 10.1109/TCE.2005.1561836.

[12] M. Hao and C. Lai, "Precoding for PAPR reduction and sidelobe suppression for NC-OFDM based cognitive radio systems," 2015 International Symposium on Intelligent Signal Processing and Communication Systems (ISPACS), 2015, pp. 542-547, doi: 10.1109/ISPACS.2015.7432831.

[13] A. S. Namitha and S. M. Sameer, "Joint PAPR and sidelobe reduction in noncontiguous OFDM based cognitive radio systems," 2015 IEEE International Conference on Signal Processing, Informatics, Communication and Energy Systems (SPICES), 2015, pp. 1-5, doi: 10.1109/SPICES.2015.7091449.

[14] Z. Wang, L. Mei, X. Wang, N. Zhang and S. Wang, "Joint suppression of PAPR and sidelobe of hybrid carrier communication system based on WFRFT," 2015 IEEE/CIC International Conference on Communications in China (ICCC), 2015, pp. 1-5, doi: 10.1109/ICCChina.2015.7448588.

[15] T. Wu and C. Chung, "Correlatively Precoded OFDM With Reduced PAPR," in IEEE Transactions on Vehicular Technology, vol. 65, no. 3, pp. 1409-1419, March 2016, doi: 10.1109/TVT.2015.2411653.

[16] M. A. Stephen, Y. K. Moorthy and S. S. Pillai, "A novel method for joint PAPR reduction and sidelobe suppression in NC-OFDM based Cognitive Radio system," 2016 International Conference on Emerging Technological Trends (ICETT), 2016, pp. 1-6, doi: 10.1109/ICETT.2016.7873730.

[17] Wei, Peng & Dan, Lilin & LI, Shaoqian. (2016). Joint Optimization of Peak-to-Average Power Ratio and Spectral Leakage in NC-OFDM. IEICE Transactions on Communications. E99.B. 10.1587/transcom.2016EBP3151.

[18] M. Hao and L. Chen, "Sidelobe power and PAPR reduction for CR systems with NC-OFDM," *2017 International Symposium on Intelligent Y. Zheng, J. Zhong, M. Zhao and M. Lei, "A low-complexity precoding technique for N-continuous OFDM," 2013 IEEE 14th Workshop on Signal Processing Advances in Wireless Communications (SPAWC), Darmstadt, Germany, 2013, pp. 644-648, doi: 10.1109/SPAWC.2013.6612129.Signal Processing and Communication Systems (ISPACS)*, 2017, pp. 50-55, doi: 10.1109/ISPACS.2017.8266444.

[19] L. Wang, L. Zhang, R. Xu and L. Peng, "Precoding for joint spectral sidelobes suppression and PAPR reduction in OFDM system," 2017 IEEE 9th International Conference on Communication Software and Networks (ICCSN), 2017, pp. 482-486, doi: 10.1109/ICCSN.2017.8230159.

[20] C. Ni, T. Jiang and W. Peng, "Joint PAPR Reduction and Sidelobe Suppression Using Signal Cancelation in NC-OFDM-Based Cognitive Radio Systems," in IEEE Transactions on Vehicular Technology, vol. 64, no. 3, pp. 964-972, March 2015, doi: 10.1109/TVT.2014.2327012.

[21] A. Tom, A. Şahin and H. Arslan, "Suppressing Alignment: Joint PAPR and Out-of-Band Power Leakage Reduction for OFDM-Based Systems," in IEEE Transactions on Communications, vol. 64, no. 3, pp. 1100-1109, March 2016, doi: 10.1109/TCOMM.2015.2512603.

[22] Yanqing, Liu & Dong, Liang. (2017). Iterative Reduction of Out-of-Band Power and Peak-to-Average Power Ratio for Noncontiguous OFDM Systems Based on POCS. IEICE Transactions on Communications. E100.B.10.1587/transcom. 2016EBP3326.

[23] Kaliki, Sravan & Golla, Shiva & Kurukundu, Rama. (2020). An optimization technique for simultaneous reduction of PAPR and out-of-

band power in NC-OFDM-based cognitive radio systems. ETRI Journal. 10.4218/etrij.2019-0255.

[24] B. Sklar, F. Harris, (2020), *Digital Communications: Fundamentals and Applications*, 3rd edition, Pearson,New York.

[25] Davis, P.J. and Rabinowitz, P. (1984) *Methods of Numerical Integration*, 2nd Edition, Academic Press, New York.

[26] C. Tellambura, "Computation of the continuous-time PAR of an OFDM signal with BPSK subcarriers," in IEEE Communications Letters, vol. 5, no. 5, pp. 185-187, May 2001, doi: 10.1109/4234.922754.

[27] K. D. Wong, M. Pun and H. V. Poor, "The continuous-time peak-to-average power ratio of OFDM signals using complex modulation schemes," in IEEE Transactions on Communications, vol. 56, no. 9, pp. 1390-1393, September 2008, doi: 10.1109/TCOMM.2008.060438.

[28] D. Qu, J. Ding, T. Jiang and X. Sun, "Detection of Noncontiguous OFDM Symbols for Cognitive Radio Systems without Out-of-Band Spectrum Synchronization," in IEEE Transactions on Wireless Communications, vol. 10, no. 2, pp. 693-701, February 2011, doi: 10.1109/TWC.2011.120810.101324.

[29] M. Lobo, L. Vandenberghe, S. Boyd, and H. Lebret, "Applications of second-order cone programming," Linear Algebra Appl., vol. 284, no. 1–3, pp. 193–228, Nov. 1998.

[30] Boyd, S., & Vandenberghe, L. (2004). Convex Optimization. Cambridge: Cambridge University Press. doi:10.1017/CBO9780511804441

[31] I. Gutman, I. Iofedov and D. Wulich, "Iterative Decoding of Iterative Clipped and Filtered OFDM Signal," in IEEE Transactions on Communications, vol. 61, no. 10, pp. 4284-4293, October 2013, doi: 10.1109/TCOMM.2013.090513.120983.

[32] 3GPP TR 38.901 version 16.1.0 Release 16, "Study on channel model for frequencies from 0.5 to 100 GHz", Nov. 2020.

[33] Y. Rahmatallah and S. Mohan, "Peak-To-Average Power Ratio Reduction in OFDM Systems: A Survey And Taxonomy," in *IEEE Communications Surveys & Tutorials*, vol. 15, no. 4, pp. 1567-1592, Fourth Quarter 2013, doi: 10.1109/SURV.2013.021313.00164.

[34] Y. Zheng, J. Zhong, M. Zhao and M. Lei, "A low-complexity precoding technique for N-continuous OFDM," *2013 IEEE 14th Workshop on Signal Processing Advances in Wireless Communications (SPAWC)*, Darmstadt, Germany, 2013, pp. 644-648, doi: 10.1109/SPAWC.2013.6612129.

[35] Ahmed K. Abed, Riyadh Mansoor and Ali K. Abed, "Particle Swarm Optimization-based dummy sub-carriers insertion for peak to average power ratio reduction in OFDM systems", *ICT Express*, vol. 8, no. 1, pp. 135-141, 2022.

[36] Khan, M., Rao, K., Amuru, S. *et al.* Low PAPR reference signal transceiver design for 3GPP 5G NR uplink. *J Wireless Com Network* **2020**, 182 (2020). https://doi.org/10.1186/s13638-020-01787-1

[37] Kumar, A. PAPR Reduction in Beyond 5G Waveforms Using a Novel SLM Algorithm. *Natl. Acad. Sci. Lett.* (2023). https://doi.org/10.1007/s40009-023-01289-w

[38] Seung Hee Han and Jae Hong Lee, "An overview of peak-to-average power ratio reduction techniques for multicarrier transmission," in *IEEE Wireless Communications*, vol. 12, no. 2, pp. 56-65, April 2005, doi: 10.1109/MWC.2005.1421929.

[39] T. Jiang and Y. Wu, "An Overview: Peak-to-Average Power Ratio Reduction Techniques for OFDM Signals," in *IEEE Transactions on Broadcasting*, vol. 54, no. 2, pp. 257-268, June 2008, doi: 10.1109/TBC.2008.915770.

[40] M. Sharif and B. H. Khalaj, "Peak to mean envelope power ratio of oversampled OFDM signals: An analytical approach", *Proc. IEEE International Conference on Communications (ICC)*, pp. 1476-1480, 2001.

[41] D. Wulich, "Comments on the peak factor of sampled and continuous signals", *IEEE Commun. Lett.*, vol. 4, no. 7, pp. 213-214, July 2000.

[42] M. Sharif, M. Gharavi-Alkhansari and B. H. Khalaj, "On the peak-to-average power of OFDM signals based on oversampling", *IEEE Trans. Commun.*, vol. 51, no. 1, pp. 72-78, January 2003.

[43] R. J. Baxley, C. Zhao and G. T. Zhou, "Constrained Clipping for Crest Factor Reduction in OFDM," in *IEEE Transactions on Broadcasting*, vol. 52, no. 4, pp. 570-575, Dec. 2006, doi: 10.1109/TBC.2006.883301.

[44] J. Armstrong, Peak-to-average power reduction for OFDM by repeated clipping and frequency domain filtering, *Electron. Lett.* 38 (5) (2002) 246–247.

[45] V. -N. Tran and T. -H. Dang, "New Clipping-and-Filtering Method for Peak-to-Average Power Ratio Reduction in OFDM," *2021 International Conference Engineering and Telecommunication (En&T)*, Dolgoprudny, Russian Federation, 2021, pp. 1-5, doi: 10.1109/EnT50460.2021.9681794.